Stem Cell Reports
Article

ISSCR

OPEN ACCESS

Human Satellite Cell Transplantation and Regeneration from Diverse Skeletal Muscles

Xiaoti Xu,[1] Karlijn J. Wilschut,[1] Gayle Kouklis,[1] Hua Tian,[1] Robert Hesse,[1] Catharine Garland,[1] Hani Sbitany,[1] Scott Hansen,[1] Rahul Seth,[2] P. Daniel Knott,[2] William Y. Hoffman,[1] and Jason H. Pomerantz[3,*]

[1]Division of Plastic and Reconstructive Surgery, Department of Surgery, University of California, San Francisco, San Francisco, CA 94143, USA
[2]Department of Otolaryngology-Head and Neck Surgery, University of California, San Francisco, San Francisco, CA 94143, USA
[3]Division of Plastic and Reconstructive Surgery, Departments of Surgery and Orofacial Sciences, Program in Craniofacial Biology, Eli and Edythe Broad Center of Regeneration Medicine, University of California, San Francisco, San Francisco, CA 94143, USA
*Correspondence: jason.pomerantz@ucsf.edu
http://dx.doi.org/10.1016/j.stemcr.2015.07.016

SUMMARY

Identification of human satellite cells that fulfill muscle stem cell criteria is an unmet need in regenerative medicine. This hurdle limits understanding how closely muscle stem cell properties are conserved among mice and humans and hampers translational efforts in muscle regeneration. Here, we report that PAX7 satellite cells exist at a consistent frequency of 2–4 cells/mm of fiber in muscles of the human trunk, limbs, and head. Xenotransplantation into mice of 50–70 fiber-associated, or 1,000–5,000 FACS-enriched $CD56^+/CD29^+$ human satellite cells led to stable engraftment and formation of human-derived myofibers. Human cells with characteristic PAX7, CD56, and CD29 expression patterns populated the satellite cell niche beneath the basal lamina on the periphery of regenerated fibers. After additional injury, transplanted satellite cells robustly regenerated to form hundreds of human-derived fibers. Together, these findings conclusively delineate a source of bona-fide endogenous human muscle stem cells that will aid development of clinical applications.

INTRODUCTION

The ability to characterize, isolate, and transplant human muscle stem cells will lay the foundation for translational efforts to regenerate or engineer human muscles. However, the absence of approaches to expand limited amounts of available tissue ex vivo with retention of stem cell properties (Montarras et al., 2005), and difficulty developing xenograft model systems to test in vivo function (Boldrin et al., 2010; Silva-Barbosa et al., 2005; Zhang et al., 2014) make it difficult to study human muscle regeneration. Consequently, endogenous human muscle stem cells have not been characterized definitively, precluding the development of clinical applications.

Muscle regeneration in mice is mediated by satellite cells that are anatomically defined based on their position between the fiber plasma membrane and the basal lamina. A subset of mouse satellite cells fulfill criteria of adult stem cells in that they engraft, proliferate, respond to injury by regenerating mature muscle, reoccupy the muscle satellite cell niche, and self-renew (Collins et al., 2005; Kuang et al., 2007; Montarras et al., 2005; Sacco et al., 2008; Sherwood et al., 2004). In contrast, satellite cell progeny can be propagated in vitro and show some capacity for differentiation, but after even brief culture cannot engraft efficiently when isolated from mouse (Montarras et al., 2005) or human (Brimah et al., 2004; Cooper et al., 2001).

To date, most attempts to transplant adult human muscle cells have used cultured derivatives of endogenous or induced muscle cells, and few used freshly isolated or prospectively identified cells. Culture-expanded human myoblasts (Skuk et al., 2010) and $CD133^+$ cells (Meng et al., 2014) can engraft and generate functional satellite cells after xenotransplantation of large numbers of cells, suggesting the potential for regenerative applications. Despite advances, the results of clinical trials (Miller et al., 1997; Partridge, 2002) and xenotransplantation experiments (Bareja et al., 2014; Castiglioni et al., 2014; Darabi et al., 2012; Ehrhardt et al., 2007; Miller et al., 1997; Partridge, 2002; Pisani et al., 2010; Silva-Barbosa et al., 2008) collectively show low transplantation efficiency, and satellite stem cell functions of self-renewal or expansion in vivo after injury have not been demonstrated from endogenous satellite cells. Thus, there is currently no established approach for directly isolating and transplanting endogenous bona-fide skeletal muscle stem cells from adult humans.

Mouse satellite cells have been well characterized (reviewed in Yin et al., 2013), providing a strong foundation for human translation. Although available evidence suggests that human and mouse satellite cells have similar morphological characteristics and surface marker expression (Boldrin et al., 2010; Kadi et al., 2004; Mackey et al., 2009), significant differences have been identified. For example, it has been suggested that the canonical satellite cell transcription factor *Pax-7* (Seale et al., 2000) is not absolutely restricted to or expressed in all human satellite cells (Reimann et al., 2004). Moreover, surface marker expression is not identical between mouse and human satellite cells (Boldrin and Morgan, 2012) and there is no accepted set of surface markers upon which to base human

satellite cell isolation. Whereas satellite cell frequency and function is heterogeneous in murine muscles (Collins et al., 2005; Kuang et al., 2007; Ono et al., 2010; Pavlath et al., 1998; Zammit, 2008), little is known about heterogeneity in human muscles. Human satellite cell heterogeneity could in theory constrain transplantation of particular recipient muscles. Finally, while direct transplantation of individual muscle fibers from mice preserves very robust satellite cell function (Collins et al., 2005; Hall et al., 2010) and bypasses flow cytometry, human fiber experimentation has not kept pace. Human fibers have been successfully cultured (Bonavaud et al., 2002) but are significantly longer than in the mouse, making them difficult to handle and deterring experimentation with them (Boldrin and Morgan, 2012). Recently, the feasibility of transplanting cultured human fiber fragments has been demonstrated (Marg et al., 2014).

Here, we report the successful transplantation of adult human muscle stem cells from diverse muscles by two distinct approaches, direct transplantation of niche-protected satellite cells on fibers and transplantation of flow-cytometry-enriched satellite cells. We analyze the frequency of satellite cells in diverse human muscles, corroborating CD29 and CD56 surface marker expression with satellite cell morphological characteristics and PAX-7 expression. Using irradiation and limited injury, we achieved efficient engraftment by fiber-derived or sorted satellite cells, and this enabled analysis of differentiation, response to injury, and self-renewal. Our results demonstrate stem cell phenotypes and establish approaches for transplantation of endogenous human satellite stem cells.

RESULTS

Human Satellite Cells Co-express PAX7, CD56, and CD29 and Exist at Predictable Frequencies in Diverse Skeletal Muscles of Adults

To investigate human satellite cell heterogeneity, we analyzed satellite cells in different human muscles. Muscle biopsies from males and females were sharply dissected during reconstructive surgery. None had systemic muscle disease and all biopsies were from healthy muscle not previously operated on. Mononucleated cells in the sublaminar position on the periphery of fixed individual fibers (satellite cells) were analyzed for expression of PAX7, CD29 (B-1 INTEGRIN), and CD56 (NCAM), which have been shown to be expressed by human satellite cells (Boldrin and Morgan, 2012; Schubert et al., 1989). Nuclear PAX7 (Figure 1A, top panels), and surface CD56 and CD29 (Figure 1A, middle and bottom panels) staining was readily detected on human satellite cells within the laminin-marked basement membrane in all biopsies (Figure 1). To determine whether satellite cell frequency is heterogeneous, we analyzed 7 different adult human skeletal muscle types in 43 patients—representing the trunk, lower limbs, and head (Figure 1B schematic; Table S1). In all but two outlier samples (5% of the total), PAX7-positive satellite cells existed at a relatively homogeneous frequency of 2–4 cells per millimeter of fiber length (Figure 1B, boxplot), with little variation within groups for one muscle type or among different muscles. We also estimated the total number of satellite cells in a given volume of muscle (Figure S1). Whereas the six analyzed body and limb muscles had similar estimated satellite cell contents, the number was significantly higher for the temporalis, a result of a greater number of fibers per unit area in that muscle. Collectively, our results indicate that under normal homeostatic conditions, most adult human skeletal muscle contains a relatively homogeneous frequency of PAX7 satellite cells per fiber and that variation in satellite cell content may be predicted based on differences in fiber area and density.

Potential heterogeneity within the satellite cell pool prompted us to analyze surface marker co-expression with PAX7. We focused on CD29 and CD56 to lay the foundation for isolation by flow cytometry. In fiber preparations, CD56, CD29, and PAX7 expression correlated closely in terms of frequency per millimeter (Table S2). We also analyzed cross sections to more definitively evaluate position and co-expression of all three markers. This showed a nearly uniform correlation of CD29 and CD56 expression in PAX7-positive cells (Figures 1C, 1D, and S2). PAX7 satellite cells had a characteristic pattern of CD56 expression concentrated on the apical surface opposite the basal lamina and adjacent to the fiber plasma membrane, whereas the CD29 pattern marked the fiber plasma membrane as well as the entire perimeter of satellite cells (Figures 1C and S2). Frequent CD29 cells were observed that did not express CD56, and these cells were also negative for PAX7 (Figure S2). Quantification of co-expression patterns showed that most PAX7 cells expressed both CD56 and CD29. Very rare PAX7 cells had one, but not both, surface markers detectable (Figure 1D). Finally, since vessel-associated cell populations within skeletal muscle have previously been shown to exhibit engraftment capacity (reviewed in Chen et al., 2012), we analyzed sections for pericyte markers to confirm that our analysis of satellite cells did not include non-satellite, vessel-associated cells. We found that $CD56^{+}/PAX7^{+}$ satellite cells do not express pericyte markers, confirming that satellite and pericyte muscle cells are distinct populations (Figure S3). We conclude that CD56 and CD29 are robust markers of human PAX7 satellite cells, which are a relatively homogeneous population with respect to these three proteins in adult healthy muscle.

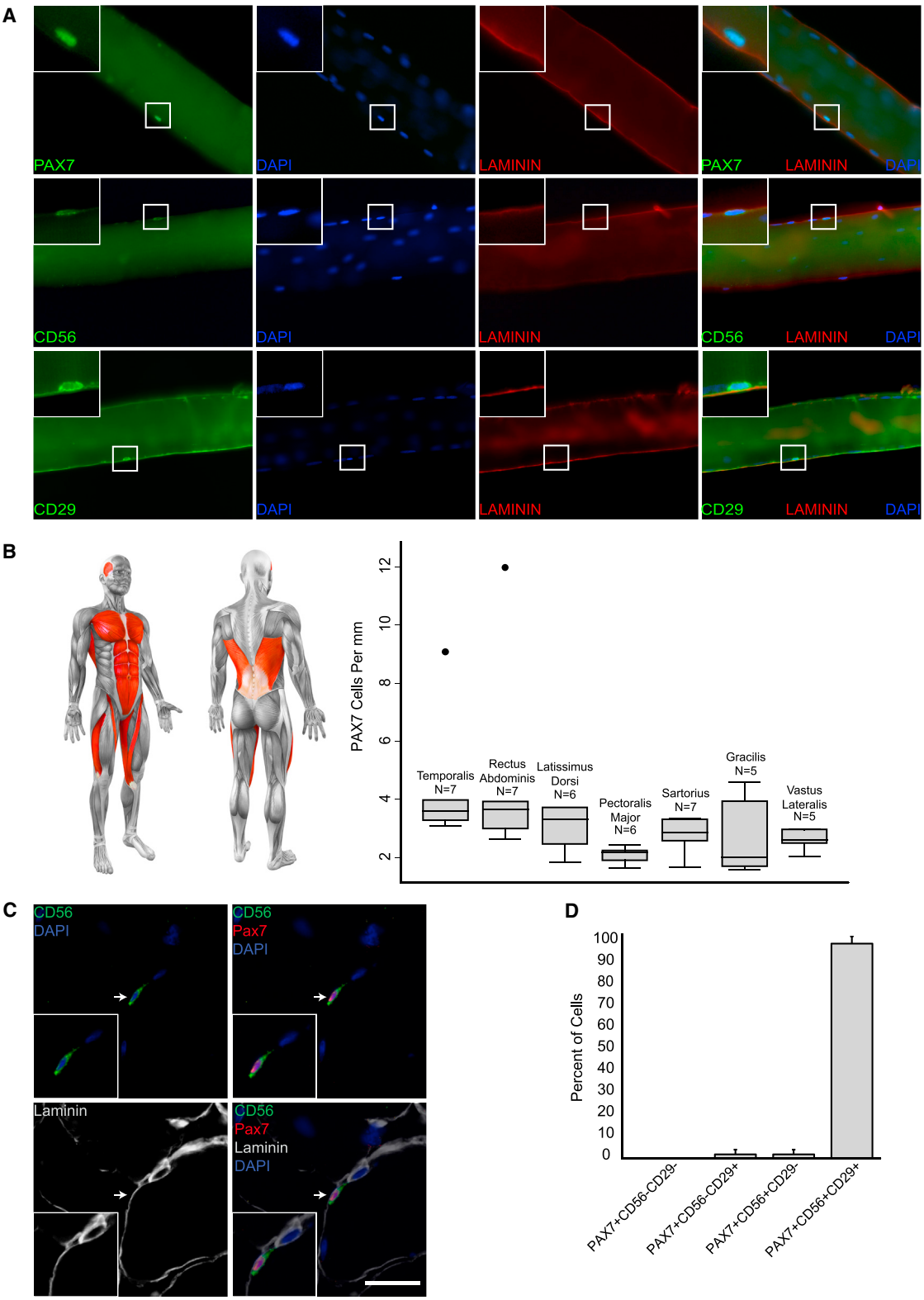

Figure 1. Characterization of Satellite Cells of Diverse Human Skeletal Muscles

(A) Representative images showing immunostaining of satellite cells on isolated fixed human fibers for PAX7 (top row), CD56 (middle row), or CD29 (Serotec) (bottom row), each with LAMININ and with DAPI. Insets: enlargement of the indicated satellite cells.

(legend continued on next page)

Evaluation of Muscle Stem Cell Function by Transplantation of Individual Human Myofibers

To evaluate human satellite cell function, we first investigated transplantation of individual myofibers, an unbiased approach independent of surface marker phenotype. We modified established techniques for fiber transplantation to work with human fibers (Bonavaud et al., 2002; Collins et al., 2005; Rosenblatt et al., 1995). Freshly prepared single live fibers yielded myoblasts in culture (Figure S4) and when fixed just after dissection satellite cell frequency (Figure 2A; Table 1; Table S3) was in accord with observations on directly fixed muscle samples (Figure 1).

Human fiber fragments (15–20 mm) were transplanted into tibialis anterior (TA) muscles of NOD SCID Gamma (NSG) mice after hindlimb irradiation (18 Gy) to incapacitate endogenous satellite cells, and notexin treatment at the time of transplantation to induce myofiber injury. Human-derived myofibers and mononucleated cells were identified by detecting human SPECTRIN and LAMIN A/C, a combination of markers that simultaneously identify human muscle fibers and human nuclei (Brimah et al., 2004). Mice were sacrificed immediately after transplantation or after 1 or 5 weeks. Immediately after transplantation, fragmented SPECTRIN staining and intact LAMIN A/C positive nuclei were identified within the TA (Figures 2B and S4B). By 1 week, human fibers had degenerated as evidenced by absence of SPECTRIN staining, and rare mononucleated LAMIN A/C positive human nuclei persisted in areas of injury surrounded by degenerating mouse fibers and mononucleated cells (Figure 2B, middle). At 5 weeks, most mouse fibers had degenerated and large clusters of human-derived fibers expressing LAMIN A/C and SPECTRIN appeared (Figure 2B, right) and were identified on sections along most of the length of the TA. Human fibers were of varying diameter with peripheral and central human nuclei and some mononucleated human cells in the interstitial space. Most SPECTRIN-positive fibers contained at least one LAMIN A/C positive nucleus within the section analyzed (see Figure 2 legend), and on serial sections LAMIN A/C nuclei could be found in virtually all SPECTRIN fibers, fulfilling human origin criteria as described in Meng et al. (2014). Fiber transplantation experiments with various donor muscles (Table 1) show that transplantation results in robust formation of human-derived fibers and that satellite cells survive, engraft, and contribute to human-derived fiber generation in excess of the original transplanted fiber over a period of weeks.

The recipient muscle was severely damaged by the radiation and notexin protocol (Figure 2D, left). To induce engraftment but minimize damage, we investigated other concomitant injury methods. Bupivacaine, a clinically used local anesthetic, induces muscle injury and regeneration upon intramuscular injection, but is less destructive than notexin (Plant et al., 2006). Transplantation of human fibers with bupivacaine into irradiated muscle resulted in successful engraftment (Figure 2C; Table 1) and much better preservation of recipient muscle architecture (Figure 2D, right). Human fiber structure was well preserved immediately after transplantation, followed by fiber degradation and retention of mononucleated LAMIN A/C cells at 1 week (Figure 2C), as with notexin. At 5 weeks, formation of human-derived muscle had occurred as clusters of SPECTRIN and LAMIN A/C fibers within intact host muscle. Transplantation of human myofibers into irradiated muscle with either notexin or bupivacaine injury demonstrates that significant fiber formation can be generated from fewer than 100 transplanted niche-protected satellite cells.

Human Satellite Cells Populate the Satellite Niche after Transplantation

To investigate human satellite cell activation and progeny during engraftment, we analyzed the expression of PAX7, MYF5, LAMININ, and human CD29 (hCD29) after fiber transplantation. Immediately after transplantation, human PAX7 cells were associated with the periphery of transplanted fibers and expressed MYF5 (Figure 3A, top row). Like satellite cells in uninjured muscle, human PAX7 cells were hCD29 positive. However, the hCD29 pattern after transplantation suggested the position on the fiber altered from tightly juxtaposed (as in Figure S2B) to a more

(B) Left: schematic of analyzed human muscles highlighted in red. Right: boxplot representation of PAX7 cell frequency per millimeter myofiber in different individuals. Boxes are grouped by muscle type. n = 5–7 individuals per group. The middle line of each boxplot indicates the median. The inner lower and upper lines represent the 25th and 75th percentile, respectively. The outer lower and upper horizontal bars represent the 25th percentile − 1.5 interquartile range and 75th percentile + 1.5 interquartile range, respectively. Black dots indicate outlier samples.

(C) Immunostaining for PAX7, CD56, and LAMININ on cross section of the vastus lateralis muscle of a 54-year-old male. Arrows indicate satellite cell expressing all three markers. Scale bar, 20 μm.

(D) Cells expressing combinations of PAX7, CD56, and CD29 in three muscle types from five individuals. The aggregate number of cells expressing each combination is presented as a percentage of total PAX7-positive cells. Bars represent the average percentage of cells for each expression pattern: PAX7^{+}CD56^{+}CD29^{+}, 96.89% ± 3.32%; PAX7^{+}CD56^{+}CD29^{-}, 1.57% ± 2.15%; PAX7^{+}CD56^{-}CD29^{+}, 1.54% ± 2.11%; PAX7^{+}CD56^{-}CD29^{-}, 0% ± 0%. Error bars, SEM.

See also Figures S1–S3 and Tables S1 and S2.

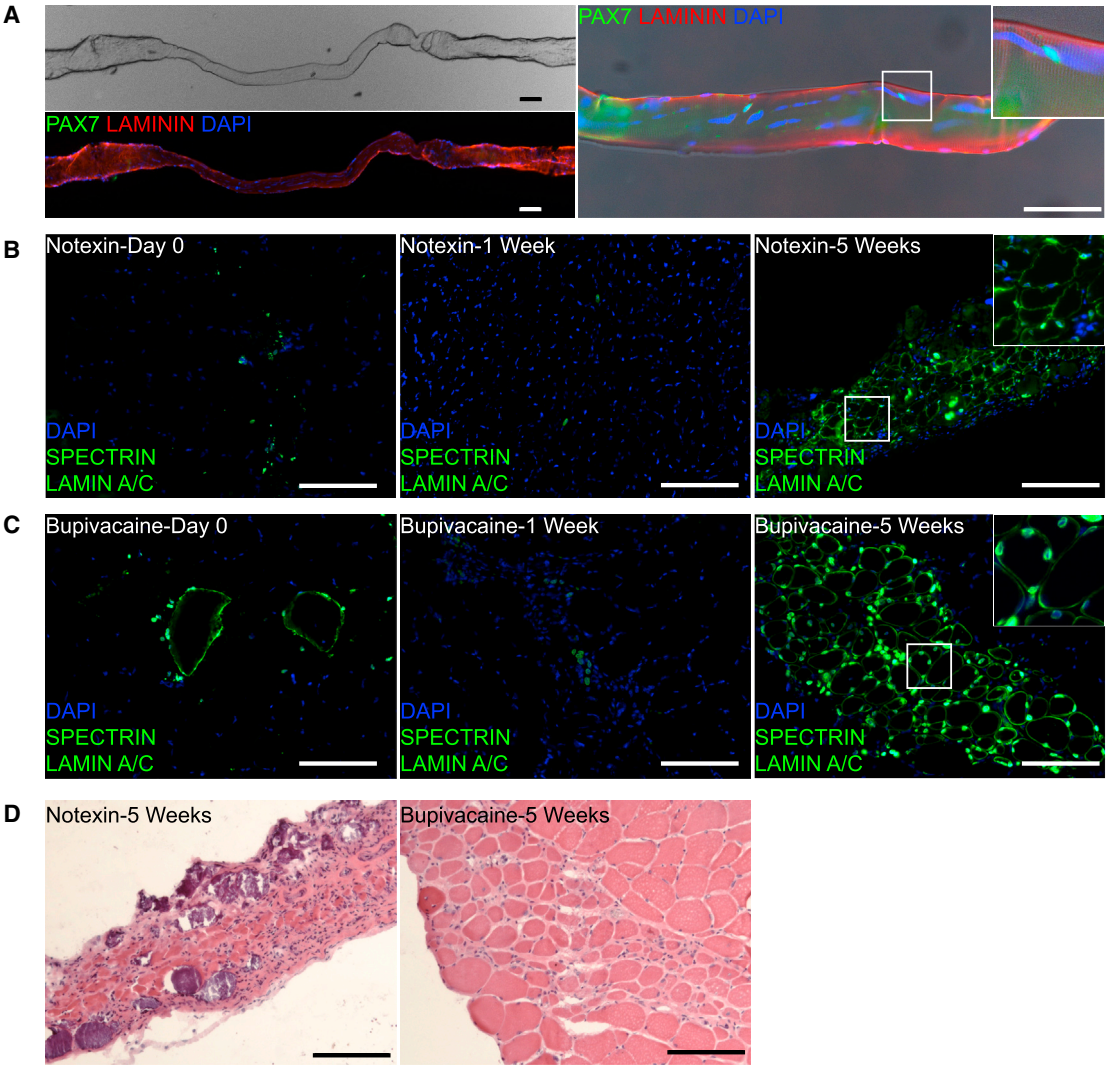

Figure 2. Satellite Cells from Isolated Live Human Muscle Fibers Engraft and Differentiate after Transplantation

(A) Myofiber isolated as in Figure S4, but fixed. Upper left: phase image of single fiber. Lower left: immunostaining of same fiber for LAMININ, PAX7, and DAPI. Right: enlarged image of the fiber with Inset showing PAX7 satellite cells, which are not visible on the lower left image.

(B) Human myofiber (vastus lateralis, 54-year-old male) transplantation into irradiated TA treated with notexin. Analysis of cross sections immunostained for human SPECTRIN and LAMIN A/C immediately after transplantation (left), at 1 week (middle) and 5 weeks (right). Inset: enlargement of the indicated area showing location of nuclei relative to fiber. Right: 46% of the human nuclei are located within fibers bound by human SPECTRIN. 70.4% (SD 9.2%, n = 3 TA muscles) of SPECTRIN-positive fibers contained a LAMIN A/C positive nucleus within the same section. On serial sections, LAMIN A/C positive nuclei could be identified within each fiber.

(C) Human myofiber (rectus abdominis, 64-year-old female) transplantation into irradiated TA treated with bupivacaine. Analysis as in (B). Right: 83.5% (SD 5.9%, n = 4 TA muscles) of SPECTRIN-positive fibers contained a LAMIN A/C positive nucleus within the same section. On serial sections, LAMIN A/C positive nuclei could be identified within each fiber.

(D) H&E of consecutive sections from 5-week samples shown in (B) and (C).

Scale bars, 100 μm. Sections were co-stained with DAPI. See also Figure S4 and Table S3.

dissociated location further from the periphery (Figure 3A, right panels). This was confirmed using LAMININ staining, which demonstrated that after fiber transplantation human PAX7 cells assumed extralaminar positions adjacent to human fibers (Figure 3A, bottom row). hCD29 expression confirmed human origin of the PAX7 cells (Figure 3A, bottom right). The expression phenotype of $PAX7^{+}/MYF5^{+}$ and extralaminar position may indicate activated satellite

Table 1. Human Myofiber Transplants

Animal	Human Muscle	Myotoxin	Length of Human Fiber Transplanted (mm)	Estimated Satellite Cells Transplanted	Human SPECTRIN Fibers
1	VL, 52M	Ntx	20	52	165
2	VL, 52M	Ntx	20	52	99
3	VL, 52M	Ntx	20	52	11
4	RA, 64F	Bup	15	70	119
5	RA, 64F	Bup	15	80	43
6	RA, 64F	Bup	15	80	38
7	RA, 64F	Bup	15	80	6
8	RA, 60F	Ntx	–	–	3
9	RA, 60F	Ntx	–	–	55
10	G, 17M	Ntx	–	–	68
11	G, 17M	none	–	–	20
12	G, 17M	none	–	–	5
13	RA, 46F	none	–	–	55
14	RA, 46F	Ntx	–	–	89
15	RA, 46F	Ntx	–	–	107
16	RA, 46F	none	–	–	8
17	S, 60M	Ntx	–	–	24
18	S, 60M	Ntx	–	–	35
19	S, 60M	Bup	–	–	5
20	S, 60M	Bup	–	–	53

For transplants in which fiber length was measured (#1–7), the length was used to estimate the number of satellite cells using the average satellite cell frequency for that particular donor muscle type (Figure 1). Engraftment was analyzed at 5 weeks. – indicates not determined. All transplants were engrafted from the five muscle types in six muscles from six individuals. Ntx, notexin; Bup, bupivacaine; RA, rectus abdominis; VL, vastus lateralis; G, gastrocnemius; S, soleus; M, male; F, female.

cells or committed progenitors similar to what has been described in mice (Kuang et al., 2007). 1 week after transplantation, $PAX7^-/MYF5^+$ was the predominant transcription factor phenotype, likely reflecting a population of committed progenitors (Figure 3B).

5 weeks after transplantation, human cells were common (Figure 2C, right) and human PAX7 cells were readily identified in the satellite cell position (Figure 3C). Sublaminar cells with high levels of PAX7 were located on the periphery of human fibers and expressed apical CD56 similar to endogenous human satellite cells (Figure 3C, top and bottom rows). Moreover, human PAX7 cells were enveloped by CD29 (Figure 3C, middle and bottom rows) in a pattern like that seen in satellite cells in human muscle biopsies (Figure S2). On sections taken at 5 weeks, 20.2% (±6.5%) of human-derived fibers had sublaminar PAX7 cells, compared to 13.8% (±3.8%) on a native human control sample. The morphology and expression phenotype of human sublaminar mononucleated cells 5 weeks after transplantation indicates that a portion of transplanted cells repopulate the satellite cell niche.

Isolation of CD56/CD29 Satellite Cells from Healthy Adult Muscle by Flow Cytometry

To evaluate satellite cell function in a defined population, we used flow cytometry to isolate satellite cells from human muscle biopsies. Expression patterns of CD56 and CD29 (Figure 1) supported a strategy based on these markers. After muscle digestion, live cells were depleted for CD31 and CD45 and cells that were singly or doubly positive for CD56 and CD29 were selected (Figures 4A and S5). Smaller populations of $CD56^+/CD29^-$ cells were identified in some muscle samples in contrast to consistent larger populations of $CD56^-/CD29^+$ and $CD56^+/CD29^+$ cells, in agreement with our findings on muscle sections. The $CD31^-/CD45^-/CD56^+/CD29^+$ population comprised about 1% of the total events and based on our immunostaining data should represent the satellite cell population. This was confirmed by amplifying *PAX7* transcripts from different human muscle cell populations (Figure 4B) and by staining sorted cells for PAX7 (Figure S5). When compared to unsorted muscle preparations, the $CD56^+/CD29^+$ population, but not the $CD56^-/CD29^+$ population, is highly enriched for *PAX7* transcripts, and the vast majority of $CD56^+/CD29^+$ cells express detectable levels of PAX7 protein, supporting use of the combination of CD56 and CD29 to isolate human satellite cells (Figure 4B).

Engraftment of Human CD56/CD29 Cells after Transplantation

To test human satellite cell function, we transplanted 1,000 to 5,000 $CD56^+/CD29^+$ cells into irradiated TA muscles. In all transplanted mice analyzed at 5 weeks (n = 24) (Table 2), recipient muscle contained clusters of human-derived myofibers with peripherally and centrally located human nuclei along the length of the muscle (Figure 4C) at levels slightly, but not significantly, higher with notexin than bupivacaine (Figure 4D).

When 5,000 cells of different populations were transplanted from the same muscle sample, only the $CD56^+/CD29^+$ fraction engrafted (Figures 4E and 4F). In $CD56^-/CD29^+$ transplants, human cells were identified in 2 out of 7 mice but existed as mononucleated cells. Rare fibers were detected in 1 out of 7 mice, probably reflecting contamination with $CD56^+/CD29^+$ cells or very limited

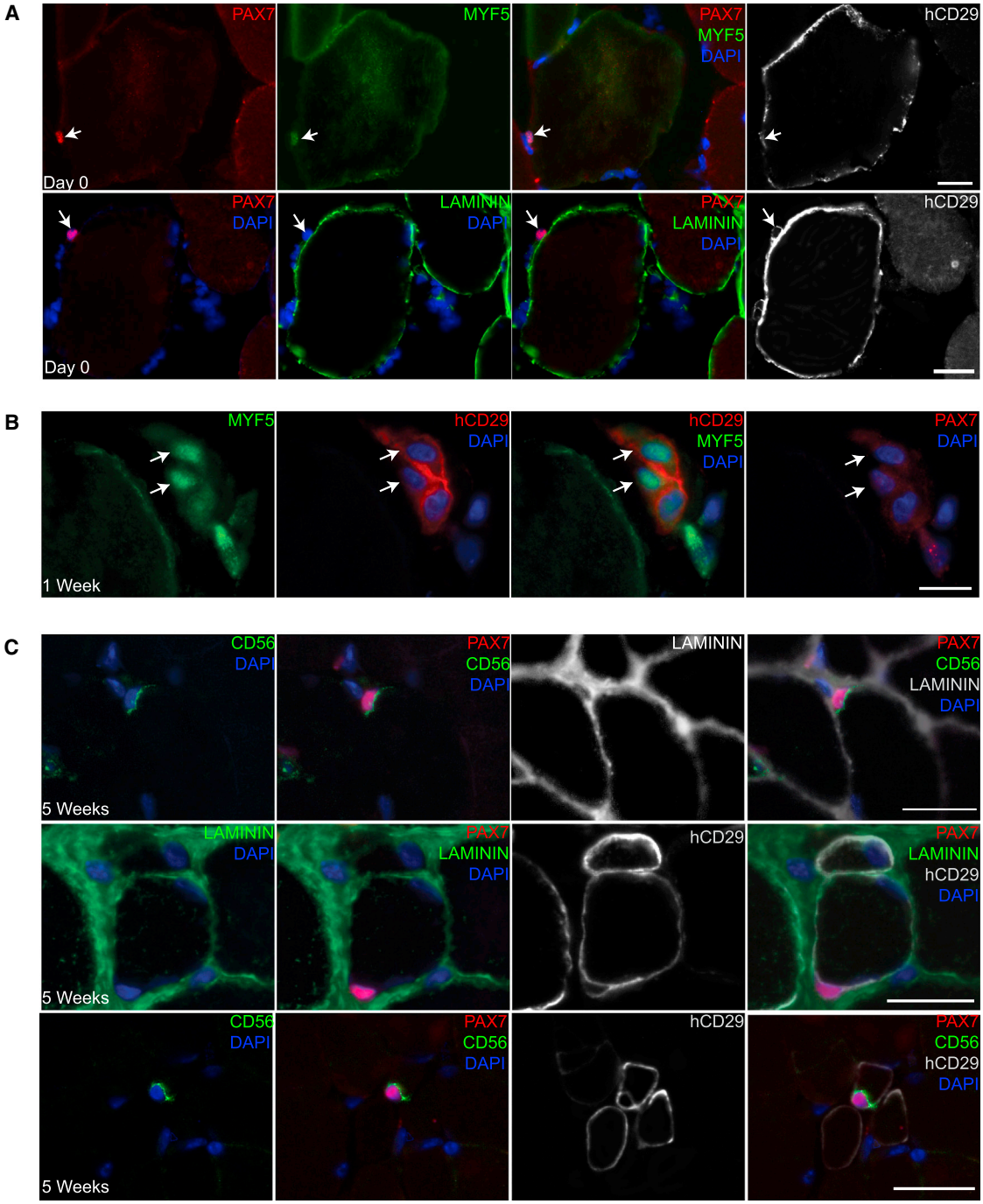

Figure 3. Analysis of Human Mononucleated Muscle Cells after fiber Transplantation

(A) Immediately after fiber injection. PAX7 cells survive and localize outside of the human fiber basement membrane. Top: immunostaining for PAX7, LAMININ, and CD29. Human cells are marked by anti-CD29 antibody (BioLegend TS2/16) (hCD29) that detects human, but not mouse, CD29 by immunostaining (see Figure S2 for antibody controls). Bottom: PAX7, MYF5, and CD29. Human PAX7 cells express MYF5 after transplantation. Arrows indicate PAX7-positive nuclei.

(B) 1 week after fiber injection. Human fibers have degenerated. Immunostaining for MYF5, hCD29, and PAX7. Surviving human cells (marked by hCD29 cy5, red pseudocolor, arrows) express MYF5. PAX7 (cy3, red pseudocolor) is not detected in these cells (right panel).

(legend continued on next page)

myogenic potential of $CD56^-/CD29^+$ cells. Transplantation of 5,000 unsorted muscle cells or passaged primary human myoblasts did not yield detectable human cells. Together, these results indicate the presence of comparable populations of satellite cells in different muscles of different individuals and show that most transplantable human satellite cells exist within the $CD56^+/CD29^+$ population.

As in fiber transplantation, transplanted human $CD56^+/CD29^+$ cells or their progeny populated the satellite cell niche and retained morphological and expression phenotypes of the parent population (Figure 4G). Sublaminar PAX7 cells were readily detected on the periphery of human fibers. Human CD29 expression confirmed human origin and apical CD56 staining was similar to that of satellite cells in human muscle (Figures 1 and S2). This replenishment of the satellite niche implies that regenerated fibers also acquired human-derived stem cell reserve capable of fiber maintenance and repair.

Transplanted Human Satellite Cells Respond to Injury by Expansion and Differentiation into Mature Human-Derived Skeletal Muscle

To evaluate whether engrafted human satellite cells can regenerate in response to injury, we performed reinjury experiments. Reinjured muscles were compared to parallel non-reinjured muscles, according to the schematic (Figure 5A). After transplantation of 5,000 $CD56^+/CD29^+$ cells with bupivacaine, expected engraftment occurred at 5 weeks (Figures 5B and 5C, left, and 5D, black triangles; Table 2). Since it has been reported that anti-human SPECTRIN can cross react with mouse fibers (Rozkalne et al., 2014), we confirmed that the SPECTRIN and LAMIN A/C staining specifically identifies human fibers by staining adjacent sections with human specific anti-DYSTROPHIN antibody, and the staining patterns correlated well (Figure S6). In mice analyzed at 10 weeks without reinjury, engrafted human cells and human fibers persisted in clusters of similar numbers of human-derived fibers comparable to that at 5 weeks (Figures 5B, middle, and 5D), but human fiber diameter increased suggesting maturation (Figure S7). Human fibers accounted for less than 5% of the overall muscle fibers at 5 weeks, and at 10 weeks without reinjury, the composition was similar (Figures 5B, middle, and 5E). Human satellite cells were identified 5 weeks after transplantation by co-staining with PAX7, LAMININ, and LAMIN A/C after (Meng et al., 2014; Skuk et al., 2010) (Figure S7F). Reinjury with notexin resulted in abundant generation of new human fibers in large groups indicating a robust proliferative response (Figures 5B, right, and 5D). After reinjury, human fiber diameter varied more than in 10-week controls (Figure S7E), and many fibers contained centrally located human nuclei. To better characterize the degree of human muscle cell regeneration, we examined longitudinal sections of reinjured TA muscles for expression of human DYSTROPHIN, LAMIN A/C, and satellite cell markers (Figure S7). The vast majority of the myonuclei in human-derived fibers were of human origin (Figures S7A and S7B), and in contrast to a patchy, domain-limited human protein expression pattern that would be expected in highly chimeric fibers (Brimah et al., 2004), human DYSTROPHIN staining was uniformly present in fibers containing LAMIN A/C positive myonuclei (Figures S7A and S7B). 10,000–20,000 human myonuclei were distributed over the length of reinjured muscles, and like in cross sections, human-derived satellite cells were identified in longitudinal sections (Figures S7C and S7D).

A significant growth advantage of engrafted human satellite cells is shown by the global replacement of the muscle with human-derived cells after reinjury (Figure 5C). This is most likely a result of the use of irradiation of the host muscle to incapacitate endogenous mouse satellite cells, as evidenced by the abundance of human-derived cells and absence of host PAX7 cells (Figure S7). At 5 weeks, small clusters of muscle express human DYSTROPHIN in contrast to a majority of mouse DYSTROPHIN-expressing fibers (Figure 5C, top row). After reinjury, most muscle fibers were of human origin, accounting for up to 100% of the muscle (Figure 5E), and they matured to the point that they expressed human DYSTROPHIN (Figures 5C, right, and 5E). Human DYSTROPHIN expression correlated with SPECTRIN and LAMIN A/C staining of adjacent sections (Figure S7G). To further evaluate maturation, we analyzed samples for neuromuscular junctions on human-derived fibers (Figure 5G). Co-staining with antibodies to SYNAPTOPHYSIN, α-BUNGAROTOXIN, and human DYSTROPHIN identified mature neuromuscular junctions by adjacent layers of SYNAPTOPHYSIN (presynaptic) and α-BUNGAROTOXIN (postsynaptic) staining on the fiber periphery. Junctions were observed on approximately 2% of human DYSTROPHIN-expressing fibers on sections after reinjury. Together, these reinjury experiments demonstrate a robust capacity of engrafted human satellite cells to expand and to generate quantities of mature muscle in excess of the original number

(C) 5 weeks after fiber injection. Human PAX7 cells occupy the satellite cell niche on new human fibers. Top row: immunostaining for PAX7, CD56, and LAMININ. Sublaminar PAX7 cell expresses apical hCD56. Middle row: PAX7, hCD29, and LAMININ. Note sublaminar PAX7 cell and marking of the satellite cell and the fiber membrane by hCD29. Bottom row: PAX7, CD56, and CD29. Human satellite cell expressing high PAX7, apical CD56, and circumferential CD29.
Sections were co-stained with DAPI. Scale bars, 20 μm. See also Figure S2.

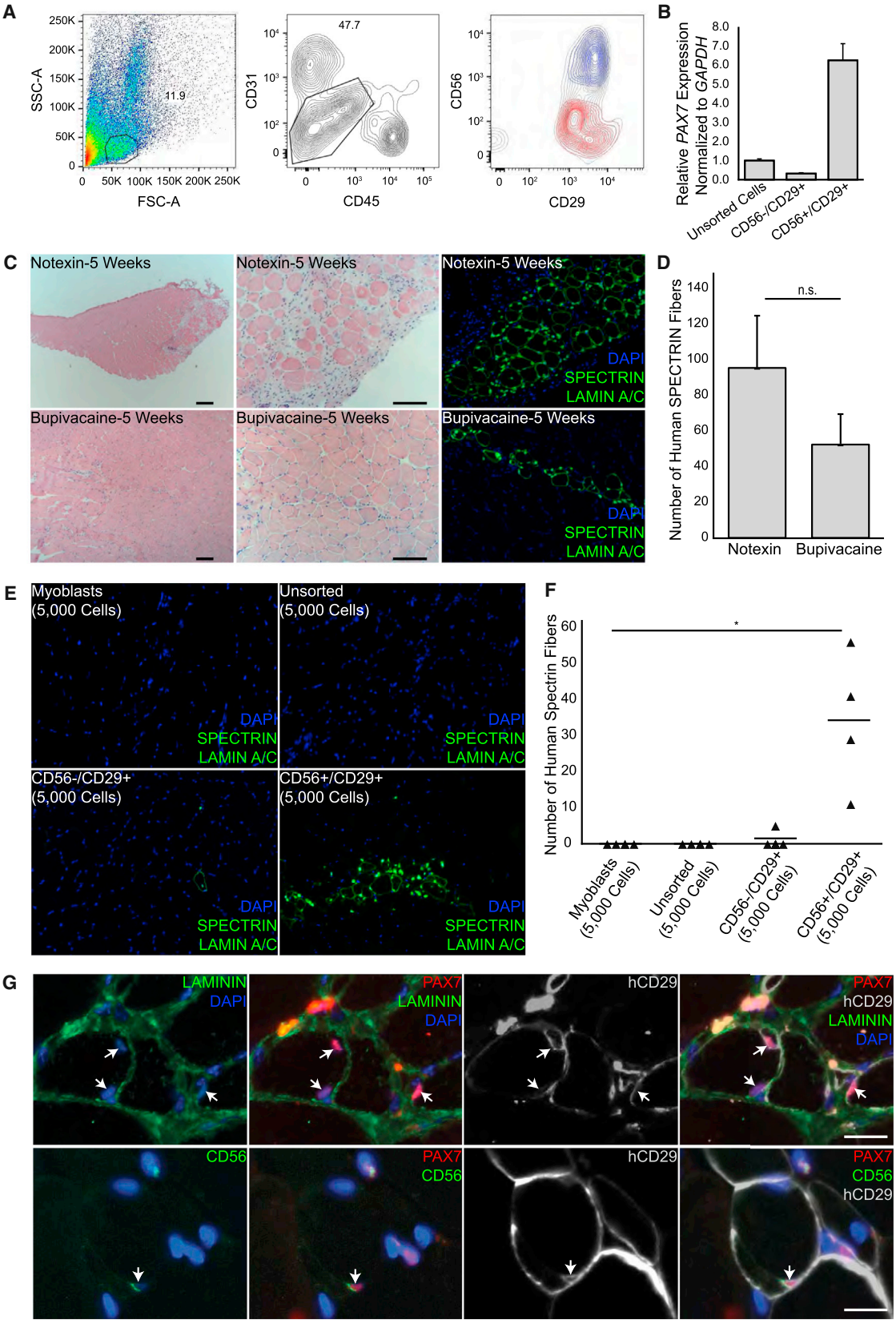

(legend on next page)

of transplanted cells, a standard criterion of a tissue stem cell.

DISCUSSION

We demonstrate that a population of adult human satellite cells fulfills conventional criteria of tissue-specific stem cells. Many characteristics of mouse satellite cells are found to be conserved in adult humans, substantiating translational approaches that extend investigations of mouse muscle regeneration. This study identifies a distinct stem cell population that can be investigated, targeted, or transplanted to treat muscle disorders.

Our analysis of satellite cell frequency in muscles of the head, trunk, and limbs suggests considerable homogeneity among different healthy human muscle types. However, when considering muscle volume, higher satellite cell content of the temporalis may relate to physiological differences of that muscle and also suggests satellite cell content may be heterogeneous in other muscles yet to be examined. Moreover, potential functional heterogeneity within the human PAX7-positive satellite cell compartment remains to be examined and important variations in satellite stem cells may yet be identified. In the two outliers we found, recent physical activity or injury may have influenced satellite cell activation and frequency as has been shown to occur in humans (Crameri et al., 2004; Mackey et al., 2009). It will be important to determine whether activated human satellite cells retain satellite stem cell properties. Our analyses demonstrate that human skeletal muscles derived from either somitic or cranial mesoderm retain an abundance of satellite cells in adulthood. It appears feasible to obtain enriched populations of relatively large numbers of satellite cells from diverse human muscles (Table S4). Our data suggest that when optimized, the yield from individual human donor muscle harvests could be expected to be adequate for regeneration of smaller recipient muscles without ex vivo expansion. The consistent engraftment that occurred after transplantation of similar numbers of fiber-associated or sorted satellite cells from six different muscle types from males and females aged 17–81 years suggests substantial diversity of potential satellite cell donor muscles. An implication of our findings is

Figure 4. Human CD56$^+$/CD29$^+$ Cells Engraft and Generate Human Muscle Fibers in Recipient Mice

(A) Representative FACS plot showing isolation of human CD31$^-$/CD45$^-$/CD56$^+$/CD29$^+$ cells prepared from the vastus lateralis muscle of an 81-year-old male. Left: forward scatterplot (FSC-A) and side scatterplot (SSC-A); gated area shown by solid line represents 11.9% of the total events. Middle: depletion of live CD45 and CD31 cells; gated area shown by solid line represents 47.7% of the cells. Right: live cells after depletion. Blue indicates CD56$^+$/CD29$^+$ selected cells; red indicates CD56$^-$/CD29$^+$ selected cells; and the backdrop indicates the total population on the CD56/CD29 plot. Cells that were CD56$^+$/CD29$^+$ or CD56$^-$/CD29$^+$ were separated for further experimentation. See also Figure S6 for isotype controls.

(B) qRT-PCR for *PAX7* expression normalized to *GAPDH* in indicated cell populations. Error bars, SEM of three replicates. Representative experiment is shown from three biological replicates.

(C) Human CD56$^+$/CD29$^+$ transplantation. Human muscle: rectus abdominis, 40-year-old female. Cross sections, 5 weeks after transplantation of 5,000 cells. Left panels: H&E. Middle panels: enlarged. Right panels: consecutive sections immunostained for human SPECTRIN and human LAMIN A/C. NSG TAs were treated with notexin (top row; n = 3 mice) and with bupivacaine (bottom row; n = 3 mice). Sections were co-stained with DAPI. Scale bars, 100 μm.

(D) Analysis of the number of human SPECTRIN fibers identified in each TA 5 weeks after transplantation with 5,000 CD56$^+$/CD29$^+$ cells. n = 3 animals for each group. Bar represents the average number of human SPECTRIN fibers for each group (bupivacaine, 52 ± 17; notexin, 95 ± 29). Statistical analysis was determined using paired Student's t tests. Error bar, SEM; n.s., not significant. 73.9% (SD 6.3%) of SPECTRIN-positive fibers in the bupivacaine samples and 78.3% (SD 3.9%) in the notexin samples contained a LAMIN A/C positive nucleus within the same section.

(E) Comparison of engraftment of different human muscle cell populations. Representative cross sections 5 weeks after transplantation of 5,000 human cells and stained for human SPECTRIN and LAMIN A/C. Sections co-stained with DAPI. Top left: cultured primary myoblasts. Top right: unsorted cells. Bottom left: CD56$^-$/CD29$^+$ cells. Bottom right: CD56$^+$/CD29$^+$ cells. All except myoblasts are from the same latissimus dorsi, 60-year-old male. n = 4 mice for each group. In the CD56$^+$/CD29$^+$ sample, 73.4% (SD 22.5%) of the SPECTRIN-positive fibers contained a LAMIN A/C positive nucleus within the same section.

(F) Dot plot showing the number of human SPECTRIN fibers (triangles) identified in each TA 5 weeks after transplantation with the indicated populations of human muscle cells. n = 4 recipient mice for each group. Myoblasts, 0 ± 0; unsorted human muscle cells, 0 ± 0; human CD56$^-$/CD29$^+$ cells, 1 ± 3; human CD56$^+$/CD29$^+$ cells, 34 ± 19. Bars represents the average number of human SPECTRIN fibers for each transplanted population. Statistical analysis was determined using paired Student's t tests. p values are * < 0.05.

(G) CD56$^+$/CD29$^+$ transplantation—analysis for human satellite cells. Cross sections from same experiment as (C) are shown 5 weeks after transplantation of 5,000 cells. Top row: human satellite cells identified by PAX7 expression and sublaminar location (LAMININ). Human origin identified by hCD29. Bottom row: human PAX7 cells retain CD29 and apical CD56 expression. Arrows indicate human satellite cells. Sections were co-stained with DAPI. Scale bar, 20 μm.

See also Figure S5 and Table S4.

Table 2. Human CD56$^+$/CD29$^+$ Satellite Cell Transplants

Animal	Human Muscle	Myotoxin	Satellite Cells Transplanted	Human SPECTRIN Fibers
1	TA, 45F	Ntx	3,500	5
2	TA, 53F	Bup	4,000	82
3	RA, 56F	Ntx	4,000	104
4	VL, 81M	Ntx	1,300	20
5	VL, 81M	Ntx	1,300	131
6	RA, 54F	Ntx	5,000	97
7	RA, 54F	Ntx	5,000	99
8	RA, 54F	Bup	5,000	2
9	RA, 54F	Bup	5,000	10
10	LD, 60M	Bup	5,000	56
11	LD, 60M	Bup	5,000	11
12	LD, 60M	Bup	5,000	29
13	LD, 60M	Bup	5,000	41
14	LD, 54M	Bup	5,000	108
15	LD, 54M	Bup	5,000	73
16	LD, 54M	Bup	5,000	112
17	LD, 54M	Bup	5,000	70
18	RA, 40F	Ntx	5,000	65
19	RA, 40F	Ntx	5,000	99
20	RA, 40F	Ntx	5,000	122
21	RA, 40F	Bup	5,000	35
22	RA, 40F	Bup	5,000	54
23	RA, 40F	Bup	5,000	68
24	RA, 64M	Bup	1,000	20

Engraftment was analyzed at 5 weeks. All transplants were engrafted from four muscle types from nine muscles of nine individuals. Ntx, notexin; Bup, bupivacaine; TA, tibialis anterior; RA, rectus abdominis; VL, vastus lateralis; LD, latissimus dorsi; M, male; F, female.

that choice of donor muscle(s) in future applications including clinical transplantation can be based on previously established criteria for human muscle expendability and donor morbidity (Mathes and Nahai, 1997) and on ease of muscle sample preparation, rather than on a muscle-specific preference based on properties of the satellite cells within it.

The different approaches to transplant satellite cells each have advantages and disadvantages from the standpoint of potential clinical application. Like in mouse experiments in which transplantation of single fibers carrying <10–20 satellite cells yield up to 100 fibers without additional injury (Collins et al., 2005; Hall et al., 2010), we found that human muscle fibers retain similarly high regenerative capacity derived from tens of satellite cells (Figure 2; Table 1) that are presumably better protected within their endogenous niche and have better preservation of surface proteins because of less enzyme exposure. Fiber transplantation also is not limited by selection of arbitrary surface markers, which could in theory exclude some stem cells. Not unlike currently used techniques of grafting adipose tissue or skin, both of which carry tissue stem cells that support graft homeostasis throughout the life of the organism, transplantation of muscle grafts (Zhang et al., 2014) is a theoretically feasible approach to regenerate small muscles that have depleted regenerative capacity. However, inherent technical difficulty complicates muscle fiber grafting.

Prospective isolation helped to better define and characterize adult human satellite cells. Our analysis of PAX7, CD56, and CD29 in adult human muscle biopsies demonstrated that the co-expression and staining pattern of CD56 and CD29, as opposed to either alone, faithfully marks PAX7-expressing satellite cells. We observed a distinct staining pattern of apical CD56 expression that was particular to sublaminar satellite cells, similar to that previously shown for M-CADHERIN (Reimann et al., 2004), which may be specific to quiescent satellite cells. It has been described previously (Lindström and Thornell, 2009) that CD56 expression can occur on PAX7-negative human mononuclear muscle cells that could represent activated satellite cells or myoblasts. The relative scarcity of this population in our study could reflect the fact that most human muscle is quiescent with little proliferation in the absence of injury. We observed a population of CD56$^+$/CD29$^+$ cells that did not stain for PAX7 on sections. It is unclear what the lineage of these cells is, but during flow cytometry, a population of CD56$^+$/CD29$^+$ cells was depleted because of co-expression of CD31. In addition to satellite cells, the myofiber and some non-muscle cells within muscle tissue also express CD29. This makes CD29, if used alone, inadequate for identification of human satellite cells. Therefore, when using CD29 to evaluate human satellite cells, CD29 must be used in conjunction with other markers such as PAX7 and LAMININ. Additionally, it is important to confirm that sublaminar CD29 staining on satellite cells is distinguished from staining of the fiber plasma membrane. Our analysis of biopsies and transplanted populations provides strong evidence that most adult muscle stem cell activity resides within the CD56$^+$/CD29$^+$ population. This study does not exclude the possibility that extralaminar PAX7 cells or rare PAX7 satellite cells that do not exhibit CD56 and CD29 co-expression have myogenic

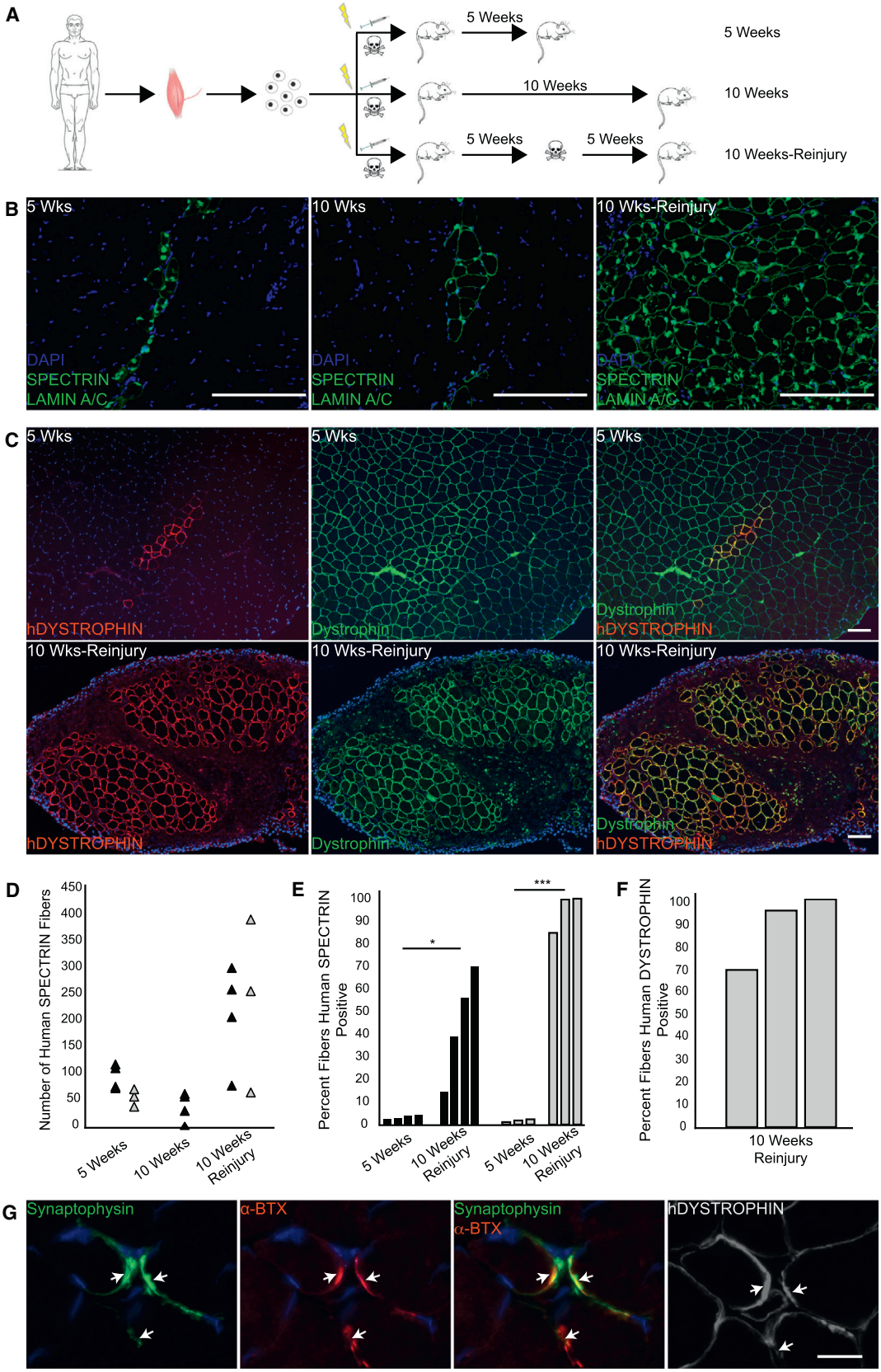

(legend on next page)

properties. Moreover, the possibility that a subpopulation of PAX7$^+$/CD56$^+$/CD29$^+$ cells can be further enriched for muscle stem cell functions merits investigation.

Engraftment, repopulation of the satellite niche, and response to additional injury clearly demonstrate that the human CD56$^+$/CD29$^+$ satellite cell population contains muscle stem cells. With respect to engraftment, our experiments resulted in a greater efficiency of human-derived fiber generation (Figures 4 and 5; Table 2) compared with other reports in which up to 100-fold greater (10^5) (Castiglioni et al., 2014) or similar (10^3) (Bareja et al., 2014) numbers of transplanted cells yielded inconsistent engraftment and lower fiber number. This discrepancy in engraftment among reports and the absence of evidence of repopulation of the niche or self-renewal in prior reports may reflect differences in cell populations studied or in the transplantation protocols such as the use of irradiation in our study, or differences in recipient mouse strains. Future improvements in isolation efficiency of CD56$^+$/CD29$^+$ satellite cells and engraftment protocols should maximize stem cell yield and function. Since the anesthetic bupivacaine is also an established agent to induce muscle injury in clinical settings (Scott et al., 2009) and may aid engraftment (this study), it is attractive for potential use in future muscle transplantation applications. Our study did not assess the potency of individual human muscle stem cells on a cell per cell basis, and definitive conclusions cannot be made about the full potential of adult human satellite cells. Such analysis is also complicated in xenotransplantation, where the severely immunocompromised host state would possibly affect muscle regeneration and therefore engraftment (Cooper et al., 2001; Ehrhardt et al., 2007). However, the robust engraftment after transplantation of tens of fiber-associated satellite cells or 1,000–5,000 sorted cells and the generation of tens of thousands of human myonuclei after reinjury suggest that the potency of human satellite cells is on par with their mouse counterparts.

With the approaches described in this paper, xenotransplantation of human muscle stem cells will be useful for evaluating differences in human muscle stem cell function in vivo in aged or diseased muscle and in response to pharmacological treatments or genetic modification. We also expect this system to be useful for comparing the regenerative capability of human-embryonic-stem-cell-derived or induced-pluripotent-stem-cell-derived muscle cells against naturally existing bona fide muscle stem cells.

In summary, we have characterized, isolated, and transplanted endogenous human satellite stem cells that can engraft, differentiate, replenish the niche, self-renew, and respond to injury. We show direct experimental evidence that in humans, muscle stem cell function resides within the satellite cell compartment and can be transferred directly within endogenous niches by fiber grafting or after isolation of satellite cells based on surface marker expression phenotype. Resident muscle stem cells in adult humans are a targetable cell population for clinical applications.

Figure 5. Engrafted CD56$^+$/CD29$^+$ Cells Respond to Additional Injury by Proliferating and Generating New Human Fibers

(A) Schematic of reinjury experiments. 5,000 human CD56$^+$/CD29$^+$ cells were transplanted with bupivacaine. One cohort was sacrificed at 5 weeks; one cohort was reinjured with notexin at 5 weeks and sacrificed at 10 weeks; and one cohort was sacrificed at 10 weeks without reinjury. Lightning bolt indicates 18 Gy irradiation; syringe indicates cell transplantation; and skull and crossbones indicates toxin.

(B) Immunostaining for human SPECTRIN and LAMIN A/C on transverse sections at 5 weeks (left), 10 weeks without reinjury (middle), and 10 weeks with notexin reinjury (right). Human muscle: latissimus dorsi, 54-year-old male. Representative sections are shown; n = 4 mice for each group. All sections were co-stained with DAPI. Scale bar, 100 μm.

(C) Immunostaining for pan DYSTROPHIN (DYSTROPHIN) and human DYSTROPHIN (hDYSTROPHIN) at 5 weeks (top row) and at 10 weeks after reinjury with notexin (bottom row). Human muscle: rectus abdominis, 40-year-old female. Representative sections are shown; n = 3 mice for each group. Sections were co-stained with DAPI. Scale bar, 100 μm.

(D) Dot plot showing the number of human SPECTRIN fibers (triangles) identified in individual recipient mice. Results are presented from separate experiments using two different donor muscles: black triangles indicate latissimus dorsi, 54-year-old male; gray triangles indicate rectus abdominis, 40-year-old female. n = 3–4 mice for each group. In the 10 week reinjury animals, 89.8% (SD 5.1%) of the SPECTRIN-positive fibers contained a LAMIN A/C positive nucleus within the same section analyzed for SPECTRIN.

(E) Percentage of total myofibers that express human SPECTRIN after transplantation with human CD56$^+$/CD29$^+$ cells. Each bar represents the percentage per mouse. Donor cells: black bars represent latissimus dorsi, 54-year-old male; gray bars represent rectus abdominis, 40-year-old female, as in (D). n = 3–4 mice for each group. Statistical analysis was determined using paired Student's t tests; p values are * < 0.05, *** < 0.001. See also Figure S4.

(F) Percentage of DYSTROPHIN-expressing fibers that express human DYSTROPHIN after reinjury. See also Figure S5.

(G) Analysis of neuromuscular junctions on human myofibers after reinjury. Neuromuscular junctions identified by SYNAPTOPHYSIN localization with α-BUNGAROTOXIN (α-BTX). Human origin of myofibers is indicated by human DYSTROPHIN. Arrows point to neuromuscular junctions. Sections were co-stained for DAPI. Scale bar, 20 μm.

See also Figures S6 and S7.

EXPERIMENTAL PROCEDURES

Human Muscle Procurement

This study was conducted under the approval of Committee on Human Research at the University of California, San Francisco (UCSF). Biopsies were obtained from individuals undergoing surgery at UCSF. Written consent was obtained from all subjects.

Animal Care and Transplantation Studies

Mice were housed in a pathogen-free facility at the UCSF. All procedures were approved and performed in accordance with the UCSF Institutional Animal Care and Use Committee. All experiments were performed using (NSG) mice (The Jackson Laboratory). Irradiation was done on the day of transplantation. Human cells or myofibers were injected along with toxin or media in 50 μl into the NSG TA after radiation.

Analysis of Human Muscle Satellite Cells

Human samples were split and fixed fibers were prepared as previously described (Boldrin and Morgan, 2012) and immunostained. The remaining portion of the sample was frozen in isopentane chilled in liquid nitrogen. Transverse 6 μm (for analysis of satellite cell markers on human muscle sections) or 10 μm (for H&E staining) sections were prepared.

Live Human Muscle Fiber Isolation and Analysis

Human muscle samples were incubated for 1 hr in 0.2% type I collagenase (Sigma-Aldrich). Individual fibers were separated using a dissecting microscope, measured for length, and then taken up in a syringe for transplantation, culture, or immunostaining.

$CD56^+/CD29^+$ Cell Sorting

Freshly harvested human muscle was digested either immediately or after overnight storage in 30% fetal bovine serum (FBS) at 4°C. Viable singlets were depleted for CD45 and CD31 expressing cells and remaining cells were sorted for $CD56^+/CD29^-$ and $CD56^+/CD29^+$ and collected. Cells to be transplanted were taken up in 50 μl of 20%FBS in DMEM supplemented with 10 μM Rho-associated protein kinase inhibitor in order to improve viability of dissociated cells (Goudenege et al., 2012).

qRT-PCR

Relative gene expression was determined from extracted RNA with primers for *PAX7* and housekeeping gene GAPDH. The cycle threshold (Ct) value for detection of gene of interest was normalized against the Ct value of GAPDH, and relative changes were calculated according the ΔΔCt method.

NSG TA Analysis

Harvested muscles were frozen in isopentane chilled in liquid nitrogen. Serial 10-μm transverse sections of the whole muscle were analyzed by immunostaining.

Statistical Analysis

Means between or across groups were compared using t tests for experiments involving two groups, or ANOVA was used when comparisons were made across more than two groups. Because the experiments were exploratory, multiple comparisons adjustments were not made. The p values are indicated by asterisks (*$p < 0.05$, **$p < 0.001$, and ***$p < 0.0001$) and NS (not significant).

See the Supplemental Experimental Procedures for details regarding antibodies, primers, fluorescence-activated cell sorting (FACS) controls, and staining procedures.

SUPPLEMENTAL INFORMATION

Supplemental Information includes Supplemental Experimental Procedures, seven figures, and four tables and can be found with this article online at http://dx.doi.org/10.1016/j.stemcr.2015.07.016.

AUTHOR CONTRIBUTIONS

X.X. designed experiments, performed the majority of the research, analyzed data, and wrote the manuscript. K.J.W., G.K., R.H., C.G., and H.T. designed and performed experiments and helped analyze data. H.S., S.H., R.S., P.D.K., and W.Y.H. acquired human muscle samples and commented on the manuscript. J.H.P. designed the research, interpreted data, oversaw the research, and wrote the manuscript.

ACKNOWLEDGMENTS

This work was funded by CIRM New Faculty Physician Scientist Award RN3-06504 and the University of California, San Francisco Program in Breakthrough Biomedical Research Opportunity Award to J.H.P. X.X. is supported by NIH training grant T32DK007573-23. We thank Nancy Hills for statistical analysis, Pamela Derish for editorial comments, Joanna Dreux for comments and figure preparation, and Stanley Tamaki for the conjugated PAX7 antibody. We gratefully acknowledge the constructive suggestions of Ophir Klein, Sarah Knox, and Jeffrey Bush and the sharing of unpublished data by Stephane Corbel and Helen M. Blau early on in the project.

Received: May 2, 2015
Revised: July 31, 2015
Accepted: July 31, 2015
Published: September 8, 2015

REFERENCES

Bareja, A., Holt, J.A., Luo, G., Chang, C., Lin, J., Hinken, A.C., Freudenberg, J.M., Kraus, W.E., Evans, W.J., and Billin, A.N. (2014). Human and mouse skeletal muscle stem cells: convergent and divergent mechanisms of myogenesis. PLoS ONE *9*, e90398.

Boldrin, L., and Morgan, J.E. (2012). Human satellite cells: identification on human muscle fibres. PLoS Curr. *3*, RRN1294.

Boldrin, L., Muntoni, F., and Morgan, J.E. (2010). Are human and mouse satellite cells really the same? J. Histochem. Cytochem. *58*, 941–955.

Bonavaud, S., Agbulut, O., D'Honneur, G., Nizard, R., Mouly, V., and Butler-Browne, G. (2002). Preparation of isolated human muscle fibers: a technical report. In Vitro Cell. Dev. Biol. Anim. *38*, 66–72.

Brimah, K., Ehrhardt, J., Mouly, V., Butler-Browne, G.S., Partridge, T.A., and Morgan, J.E. (2004). Human muscle precursor cell regeneration in the mouse host is enhanced by growth factors. Hum. Gene Ther. *15*, 1109–1124.

Castiglioni, A., Hettmer, S., Lynes, M.D., Rao, T.N., Tchessalova, D., Sinha, I., Lee, B.T., Tseng, Y.H., and Wagers, A.J. (2014). Isolation of progenitors that exhibit myogenic/osteogenic bipotency in vitro by fluorescence-activated cell sorting from human fetal muscle. Stem Cell Reports *2*, 92–106.

Chen, C.W., Corselli, M., Péault, B., and Huard, J. (2012). Human blood-vessel-derived stem cells for tissue repair and regeneration. J. Biomed. Biotechnol. *2012*, 597439.

Collins, C.A., Olsen, I., Zammit, P.S., Heslop, L., Petrie, A., Partridge, T.A., and Morgan, J.E. (2005). Stem cell function, self-renewal, and behavioral heterogeneity of cells from the adult muscle satellite cell niche. Cell *122*, 289–301.

Cooper, R.N., Irintchev, A., Di Santo, J.P., Zweyer, M., Morgan, J.E., Partridge, T.A., Butler-Browne, G.S., Mouly, V., and Wernig, A. (2001). A new immunodeficient mouse model for human myoblast transplantation. Hum. Gene Ther. *12*, 823–831.

Crameri, R.M., Langberg, H., Magnusson, P., Jensen, C.H., Schrøder, H.D., Olesen, J.L., Suetta, C., Teisner, B., and Kjaer, M. (2004). Changes in satellite cells in human skeletal muscle after a single bout of high intensity exercise. J. Physiol. *558*, 333–340.

Darabi, R., Arpke, R.W., Irion, S., Dimos, J.T., Grskovic, M., Kyba, M., and Perlingeiro, R.C. (2012). Human ES- and iPS-derived myogenic progenitors restore DYSTROPHIN and improve contractility upon transplantation in dystrophic mice. Cell Stem Cell *10*, 610–619.

Ehrhardt, J., Brimah, K., Adkin, C., Partridge, T., and Morgan, J. (2007). Human muscle precursor cells give rise to functional satellite cells in vivo. Neuromuscul. Disord. *17*, 631–638.

Goudenege, S., Lebel, C., Huot, N.B., Dufour, C., Fujii, I., Gekas, J., Rousseau, J., and Tremblay, J.P. (2012). Myoblasts derived from normal hESCs and dystrophic hiPSCs efficiently fuse with existing muscle fibers following transplantation. Mol. Ther. *20*, 2153–2167.

Hall, J.K., Banks, G.B., Chamberlain, J.S., and Olwin, B.B. (2010). Prevention of muscle aging by myofiber-associated satellite cell transplantation. Sci. Transl. Med. *2*, 57ra83.

Kadi, F., Charifi, N., Denis, C., and Lexell, J. (2004). Satellite cells and myonuclei in young and elderly women and men. Muscle Nerve *29*, 120–127.

Kuang, S., Kuroda, K., Le Grand, F., and Rudnicki, M.A. (2007). Asymmetric self-renewal and commitment of satellite stem cells in muscle. Cell *129*, 999–1010.

Lindström, M., and Thornell, L.E. (2009). New multiple labelling method for improved satellite cell identification in human muscle: application to a cohort of power-lifters and sedentary men. Histochem. Cell Biol. *132*, 141–157.

Mackey, A.L., Kjaer, M., Charifi, N., Henriksson, J., Bojsen-Moller, J., Holm, L., and Kadi, F. (2009). Assessment of satellite cell number and activity status in human skeletal muscle biopsies. Muscle Nerve *40*, 455–465.

Marg, A., Escobar, H., Gloy, S., Kufeld, M., Zacher, J., Spuler, A., Birchmeier, C., Izsvák, Z., and Spuler, S. (2014). Human satellite cells have regenerative capacity and are genetically manipulable. J. Clin. Invest. *124*, 4257–4265.

Mathes, S.J., and Nahai, F. (1997). Reconstructive Surgery: Principles, Anatomy and Technique (Quality Medical Publishing).

Meng, J., Chun, S., Asfahani, R., Lochmuller, H., Muntoni, F., and Morgan, J. (2014). Human skeletal muscle-derived CD133(+) cells form functional satellite cells after intramuscular transplantation in immunodeficient host mice. Mol. Ther. *22*, 1008–1017.

Miller, R.G., Sharma, K.R., Pavlath, G.K., Gussoni, E., Mynhier, M., Lanctot, A.M., Greco, C.M., Steinman, L., and Blau, H.M. (1997). Myoblast implantation in Duchenne muscular dystrophy: the San Francisco study. Muscle Nerve *20*, 469–478.

Montarras, D., Morgan, J., Collins, C., Relaix, F., Zaffran, S., Cumano, A., Partridge, T., and Buckingham, M. (2005). Direct isolation of satellite cells for skeletal muscle regeneration. Science *309*, 2064–2067.

Ono, Y., Boldrin, L., Knopp, P., Morgan, J.E., and Zammit, P.S. (2010). Muscle satellite cells are a functionally heterogeneous population in both somite-derived and branchiomeric muscles. Dev. Biol. *337*, 29–41.

Partridge, T. (2002). Myoblast transplantation. Neuromuscul. Disord. *12* (*Suppl 1*), S3–S6.

Pavlath, G.K., Thaloor, D., Rando, T.A., Cheong, M., English, A.W., and Zheng, B. (1998). Heterogeneity among muscle precursor cells in adult skeletal muscles with differing regenerative capacities. Dev. Dyn. *212*, 495–508.

Pisani, D.F., Dechesne, C.A., Sacconi, S., Delplace, S., Belmonte, N., Cochet, O., Clement, N., Wdziekonski, B., Villageois, A.P., Butori, C., et al. (2010). Isolation of a highly myogenic CD34-negative subset of human skeletal muscle cells free of adipogenic potential. Stem Cells *28*, 753–764.

Plant, D.R., Colarossi, F.E., and Lynch, G.S. (2006). Notexin causes greater myotoxic damage and slower functional repair in mouse skeletal muscles than bupivacaine. Muscle Nerve *34*, 577–585.

Reimann, J., Brimah, K., Schröder, R., Wernig, A., Beauchamp, J.R., and Partridge, T.A. (2004). Pax7 distribution in human skeletal muscle biopsies and myogenic tissue cultures. Cell Tissue Res. *315*, 233–242.

Rosenblatt, J.D., Lunt, A.I., Parry, D.J., and Partridge, T.A. (1995). Culturing satellite cells from living single muscle fiber explants. In Vitro Cell. Dev. Biol. Anim. *31*, 773–779.

Rozkalne, A., Adkin, C., Meng, J., Lapan, A., Morgan, J.E., and Gussoni, E. (2014). Mouse regenerating myofibers detected as false-positive donor myofibers with anti-human spectrin. Hum. Gene Ther. *25*, 73–81.

Sacco, A., Doyonnas, R., Kraft, P., Vitorovic, S., and Blau, H.M. (2008). Self-renewal and expansion of single transplanted muscle stem cells. Nature *456*, 502–506.

Schubert, W., Zimmermann, K., Cramer, M., and Starzinski-Powitz, A. (1989). Lymphocyte antigen Leu-19 as a molecular marker of

regeneration in human skeletal muscle. Proc. Natl. Acad. Sci. USA *86*, 307–311.

Scott, A.B., Miller, J.M., and Shieh, K.R. (2009). Treating strabismus by injecting the agonist muscle with bupivacaine and the antagonist with botulinum toxin. Trans. Am. Ophthalmol. Soc. *107*, 104–109.

Seale, P., Sabourin, L.A., Girgis-Gabardo, A., Mansouri, A., Gruss, P., and Rudnicki, M.A. (2000). Pax7 is required for the specification of myogenic satellite cells. Cell *102*, 777–786.

Sherwood, R.I., Christensen, J.L., Conboy, I.M., Conboy, M.J., Rando, T.A., Weissman, I.L., and Wagers, A.J. (2004). Isolation of adult mouse myogenic progenitors: functional heterogeneity of cells within and engrafting skeletal muscle. Cell *119*, 543–554.

Silva-Barbosa, S.D., Butler-Browne, G.S., Di Santo, J.P., and Mouly, V. (2005). Comparative analysis of genetically engineered immunodeficient mouse strains as recipients for human myoblast transplantation. Cell Transplant. *14*, 457–467.

Silva-Barbosa, S.D., Butler-Browne, G.S., de Mello, W., Riederer, I., Di Santo, J.P., Savino, W., and Mouly, V. (2008). Human myoblast engraftment is improved in laminin-enriched microenvironment. Transplantation *85*, 566–575.

Skuk, D., Paradis, M., Goulet, M., Chapdelaine, P., Rothstein, D.M., and Tremblay, J.P. (2010). Intramuscular transplantation of human postnatal myoblasts generates functional donor-derived satellite cells. Mol. Ther. *18*, 1689–1697.

Yin, H., Price, F., and Rudnicki, M.A. (2013). Satellite cells and the muscle stem cell niche. Physiol. Rev. *93*, 23–67.

Zammit, P.S. (2008). All muscle satellite cells are equal, but are some more equal than others? J. Cell Sci. *121*, 2975–2982.

Zhang, Y., King, O.D., Rahimov, F., Jones, T.I., Ward, C.W., Kerr, J.P., Liu, N., Emerson, C.P., Jr., Kunkel, L.M., Partridge, T.A., and Wagner, K.R. (2014). Human skeletal muscle xenograft as a new preclinical model for muscle disorders. Hum. Mol. Genet. *23*, 3180–3188.

Stem Cell Reports

Supplemental Information

Human Satellite Cell Transplantation and Regeneration from Diverse Skeletal Muscles

Xiaoti Xu, Karlijn J. Wilschut, Gayle Kouklis, Hua Tian, Robert Hesse, Catharine Garland, Hani Sbitany, Scott Hansen, Rahul Seth, P. Daniel Knott, William Y. Hoffman, and Jason H. Pomerantz

Supplemental Figures

Figure S1

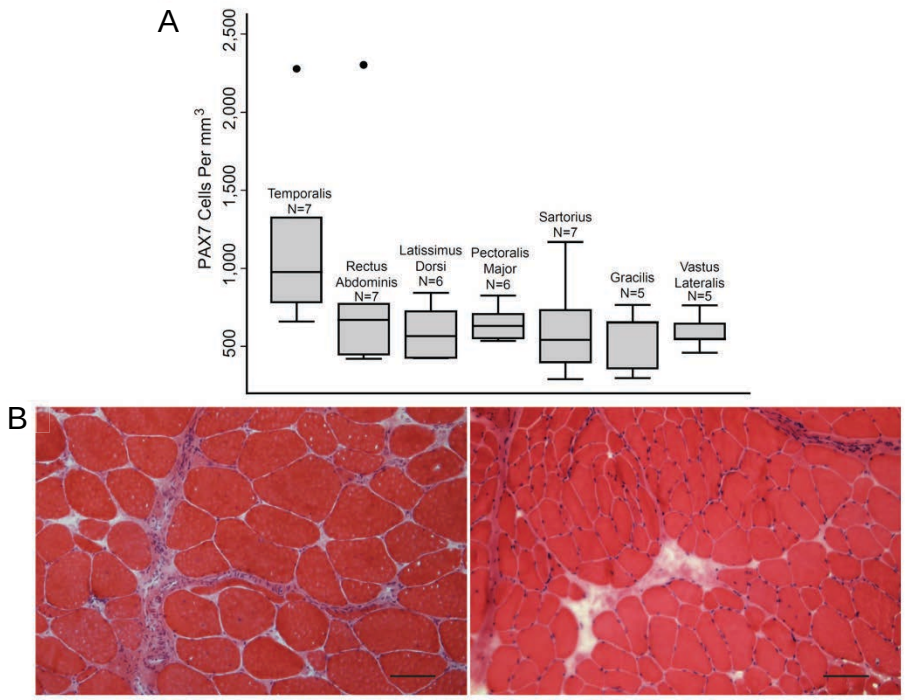

Figure S1 (related to Figure 1): Estimated PAX7 cell content per mm^3 of diverse human skeletal muscles.

A) Box plot represents the number of PAX7 cells per mm^3 volume of tissue for each sample. Boxes are grouped by muscle type. The PAX7 cell content of each sample was calculated by the following formula: PAX7 cells per mm^3 = number of myofibers per mm^2 x PAX7 cell frequency per mm myofiber. Values used in calculation and resulting PAX7 cell content for each sample are shown in Table S1. N=5-7 muscles per group. The middle line of each boxplot indicates the median, the lower and upper lines represent the 25th and 75th percentile, respectively. The outer lower and higher horizontal bars represent the 25th percentile – 1.5 interquartile range and 75th percentile +1.5 interquartile range, respectively. Black dots indicate outlier samples.

B) Representative H&E sections showing variation in number of myofibers per mm^2. Left panel is a representative section of the rectus abdominis muscle of a 56-year-old man. Right panel is

a representative section of the temporalis muscle of a 54-year-old man. Scale bar represents 100μm.

Figure S2

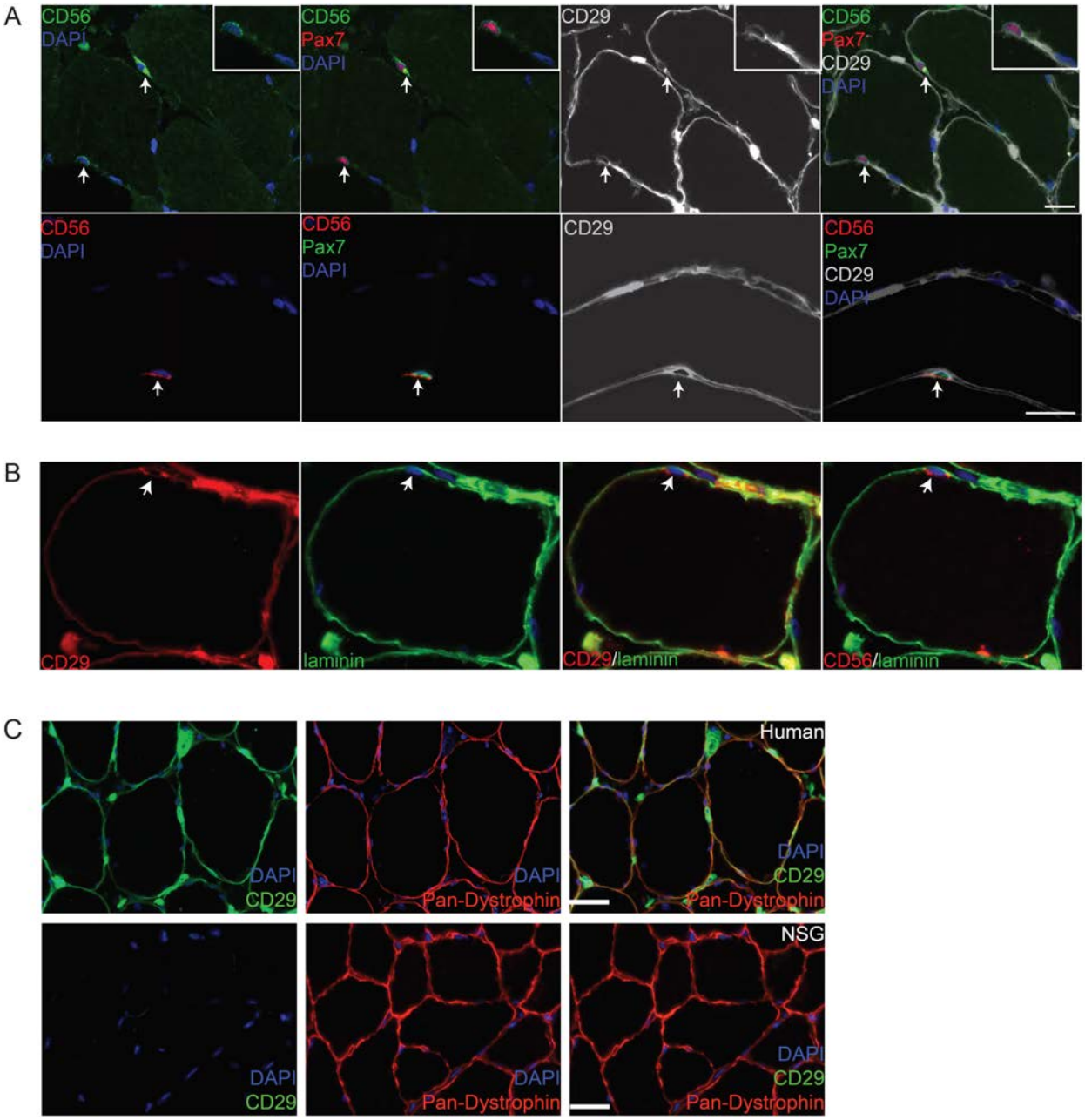

Figure S2 (related to Figure 1): Human PAX7/CD56 positive satellite cells and human skeletal muscle fibers express CD29.

A) Representative sections of human skeletal muscle showing identification of satellite cells using antibodies for PAX7, CD56 and CD29. Top and bottom rows show representative cross and longitudinal sections, respectively. Top row: Two CD56+/PAX7+ satellite cells (arrows top

left panel) are present in the section (first and second panels). Inset shows enlarged image of the satellite cell indicated by lower arrow. Human specific mouse anti-CD29 marks satellite cells, fibers, and interstitial cells. Bottom row: One satellite cell shown on longitudinal section (arrow). CD29 marks adjacent fiber membranes in addition to the satellite cell membrane (right two panels).

B) Representative section demonstrating the relationship between Laminin and CD29 on human satellite cells and fibers. (Left) Human CD29 marks the fiber as well as the circumference of the satellite cell (arrow). (Second panel from left) Laminin marks the basal lamina and clearly shows the sublaminar position of the satellite cell. (Third panel from left) The satellite cell is circumferentially marked by CD29 as opposed to Laminin which labels the basement membrane. (Fourth panel from left) CD56 marks the satellite cell with surface staining that is preferential to the apical surface adjacent to the fiber.

Scale bars – 20µm.

C) Control immunostaining panels confirming human specificity of BioLegend anti-human CD29 antibody TS2/16. Top panels show a section from a human latissimus muscle stained using the BioLegend anti-human CD29 antibody TS2/16 and counterstained with DAPI and pan-Dystrophin. Scale bar – 50µm. Bottom panels show a section from an NSG TA muscle stained with the same antibodies. Scale bar - 25µm. The staining for each sample was done side-by-side and the images were taken at the same time with identical exposures and image processing.

Figure S3

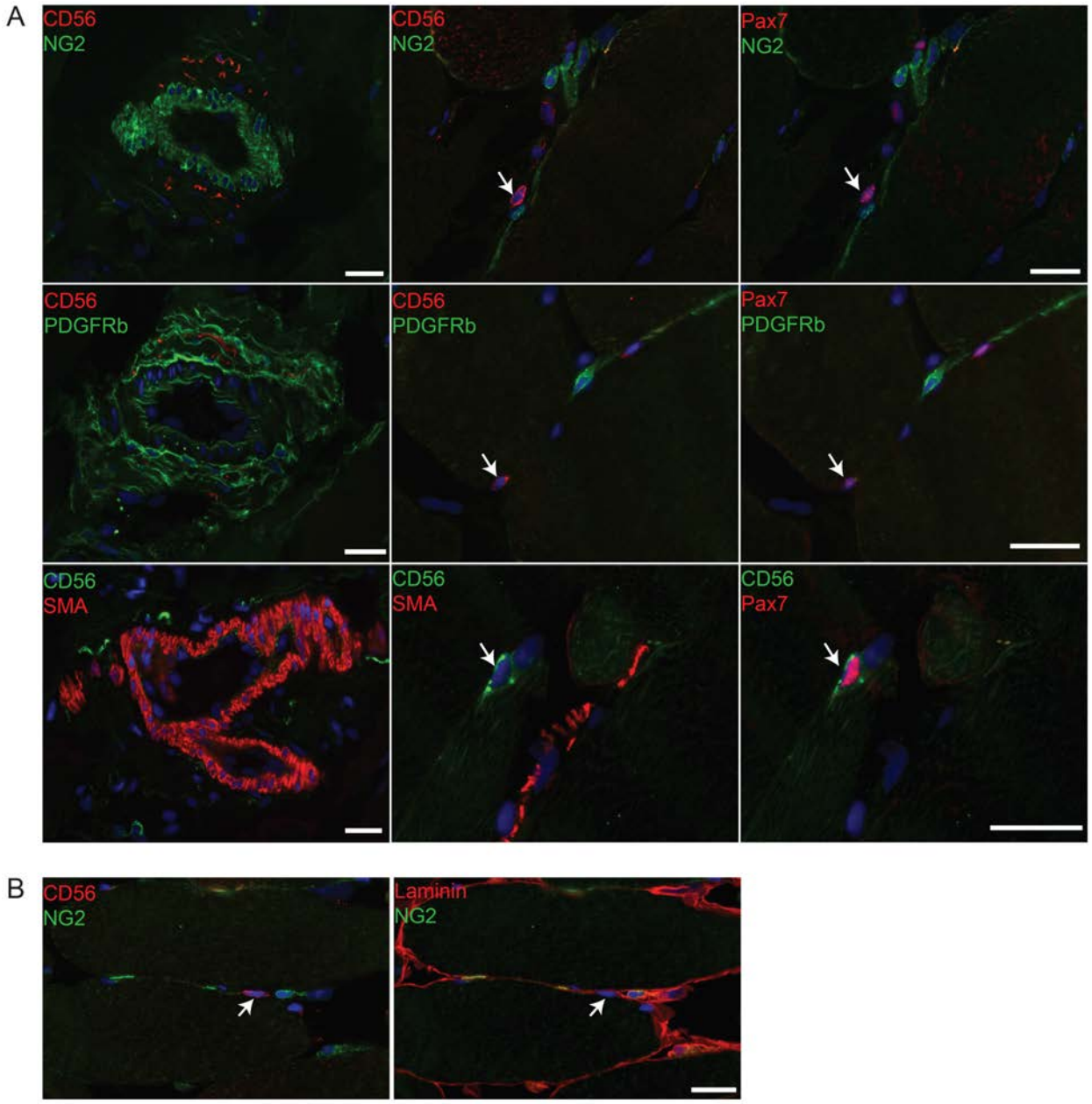

Figure S3 (related to figure 1): Satellite cells are distinct and distinguishable from pericytes and vessel associated cells.

A) Representative sections of human skeletal muscle showing the relationship of CD56+/PAX7+ satellite cells to cells expressing various pericyte markers. Top row: NG2**.** Left – typical NG2 staining pattern in a vessel within human muscle. Middle and right – CD56+/PAX7+ cell (arrow)

does not express NG2 in contrast to the NG2+ cells on the section that do not express CD56 or PAX7. Middle row: PDGFRb. Left - typical PDFRb staining pattern in a vessel within human muscle. Middle and right – CD56+/PAX7+ cell (arrow) does not express PDGFRb in contrast to the PDGFRb+ cells on the section that do not express CD56 or PAX7. Bottom Row: SMA. Left - typical SMA staining pattern in a vessel within human muscle. Middle and right – CD56+/PAX7+ cell (arrow) does not express SMA in contrast to the SMA+ cells on the section that do not express CD56 or PAX7.

B) Representative section confirming sublaminar location of CD56+ satellite cell (arrow) that does not express NG2, in contrast to the extralaminar NG2 cells which are CD56 negative.

Scale bars – 20μm.

Figure S4

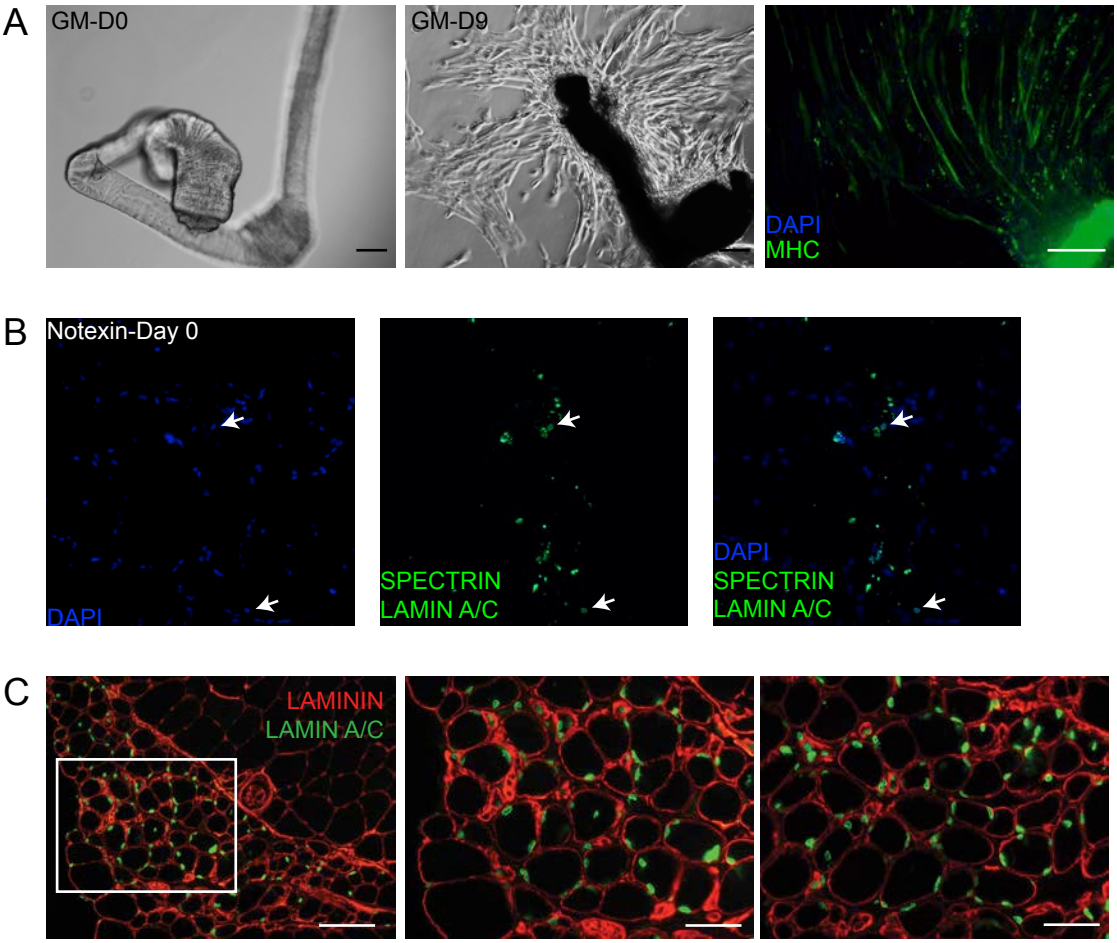

Figure S4 (related to Figure 2): Characterization of progeny cells from isolated live human muscle fibers in culture and after transplantation

(A) Left - Phase image of a single live myofiber from the rectus abdominis of a 64-year-old woman immediately after isolation. Middle - Phase image of a contracted single myofiber in GM for 9 days with multiple progeny cells. Right - Immunostaining for myosin heavy chain (MHC) in progeny cells from a single myofiber after 7 days in DM. GM - growth medium; DM - differentiation medium. Scale bars – 20µm

(B) Separate channels shown for Figure 2B left hand panel to facilitate identification of human nuclei at Day 0. Two examples of human LAMIN A/C positive, DAPI positive nuclei are marked

with arrows. Others can be readily identified in this section. The remainder of the green staining that is non-nuclear is specific SPECTRIN / LAMIN A/C staining of cell fragments.

(C) Images of adjacent sections to those shown in Figure 2C, right, stained for LAMININ and human LAMIN A/C. Left – Area of human cell engraftment. White box indicates field shown in middle panel. Scale bar – 200µm. Middle – Higher magnification image showing human derived nuclei within and outside of the LAMININ marked basal lamina. Scale bar – 100µm. Right – A second representative area. Scale bar – 100µm. Of a total of 227 nuclei counted from four different fields, 82% of the human nuclei are positioned within the basal lamina, and 18% are located in the interstitial space.

Figure S5

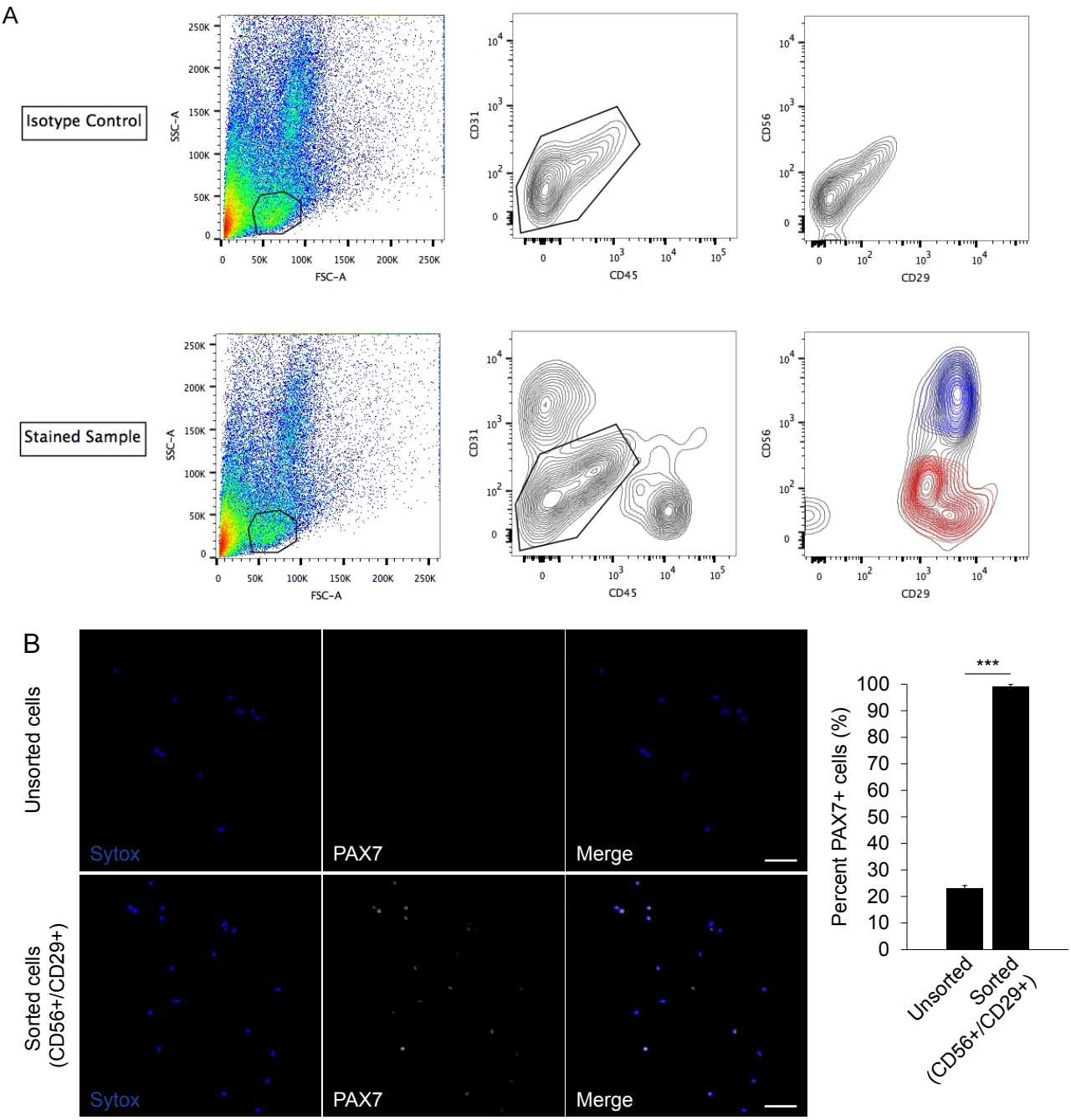

Figure S5 (related to Figure 4) Isotype controls for FACS sorting, and Pax7 immunostaining of sorted CD56/CD29 cells.

A) Top panels show isotype controls. Non-specific binding is insignificant. Lower panels – same plots as in Figure 4 for reference.

B) Pax7 immunostaining of sorted CD56/CD29 cells and unsorted cells. Cells were prepared from the vastus lateralis muscle of an 84 year old male. Top row - cells collected after muscle sample digestion prior to sorting (unsorted cells) Bottom row – CD56+/CD29+ sorted cells. All cells were counterstained with Sytox. Anti-Pax7 antibody was purified from hybridoma (DSHB) supernatant and directly conjugated using Alexa-fluor-350. Confocal images were taken and pseudocolored. Scale bar 50μm. Right – Percentage of cells in each sample that stained positive for Pax7. Student's t-test was used for statistical analysis of 20 fields counted for each condition.

Figure S6

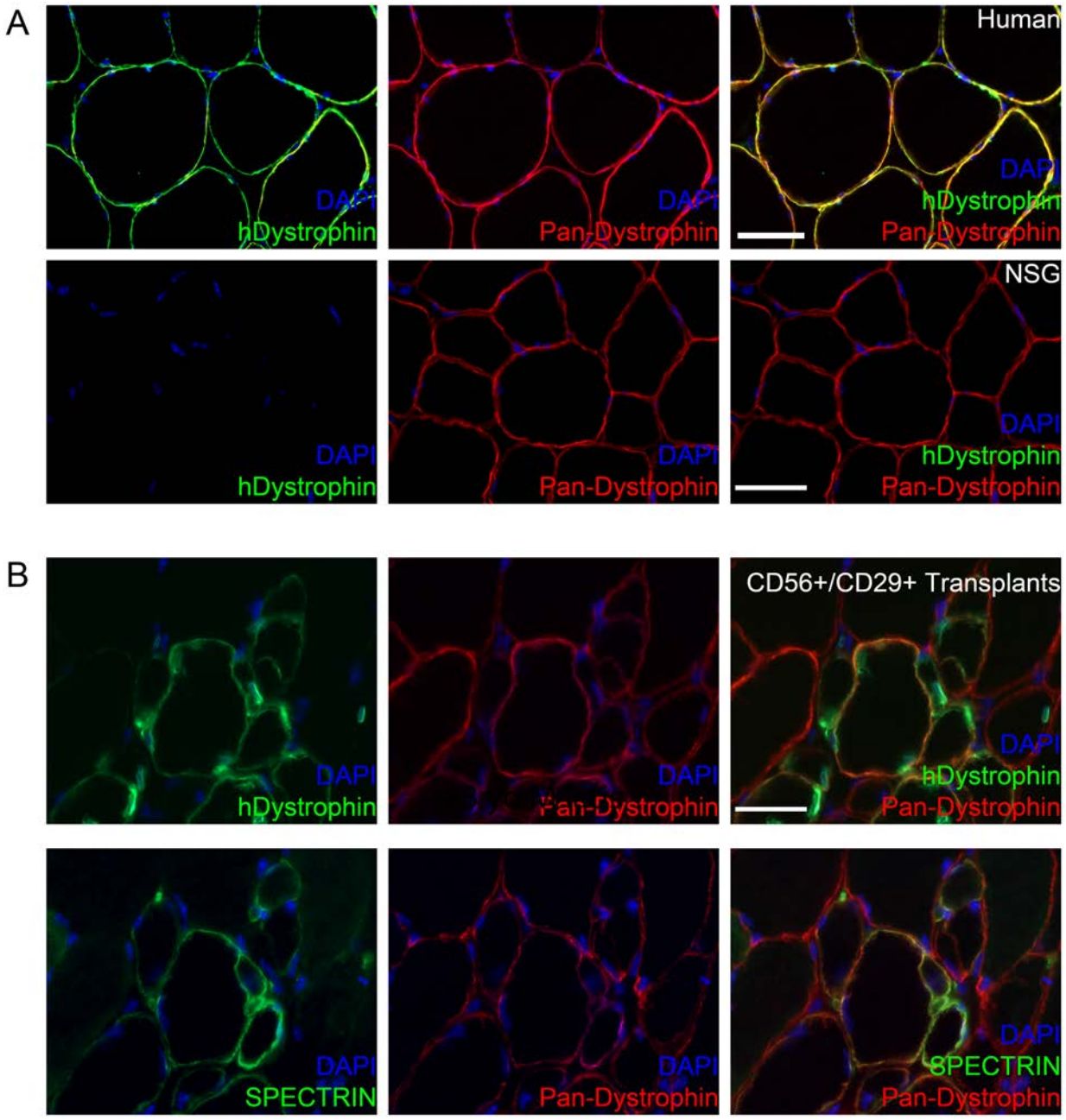

Figure S6 (related to Figure 5): Antibody controls.

A) Controls for human specificity of Leica DYS3 anti human Dystrophin**.** Immunostained frozen sections of Top - latissimus dorsi muscle (83 y/o male) and Bottom – NSG mouse TA muscle.

Pan – Dystrophin used as counter stain to show presence of muscle fibers. Scale bar top 50µm, bottom 25µm.

B) Comparison of human Dystrophin staining pattern with Spectrin on adjacent sections. Adjacent sections were taken from a TA muscle harvested 5 weeks after transplantation with 5,000 CD56+/CD29+ cells (same experiment as shown in Figure 5B). Top row- section stained with human and pan dystrophin antibodies. Bottom row – adjacent section stained with human Spectrin antibody and pan-dystrophin.

Figure S7

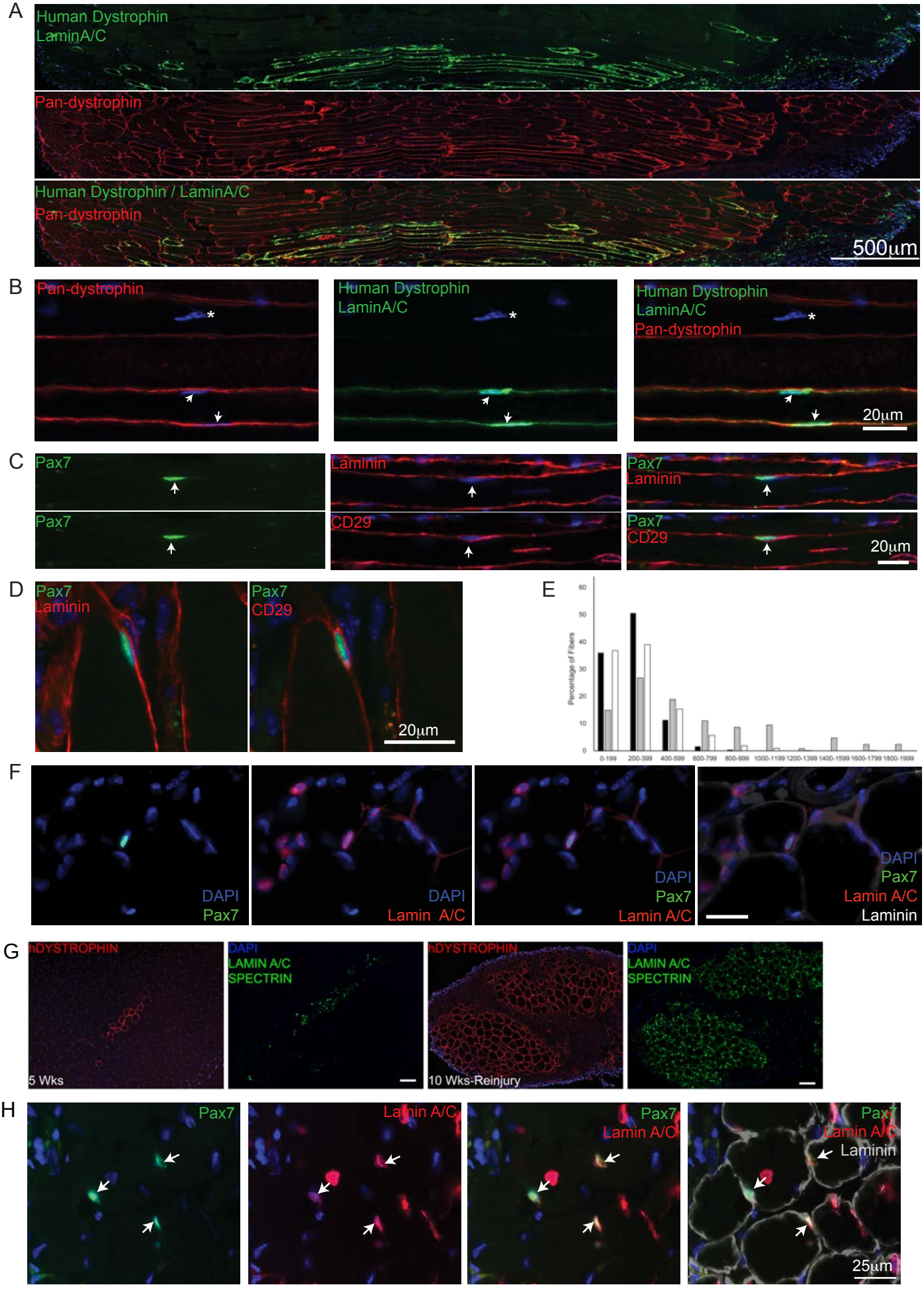
A
Human Dystrophin
LaminA/C
Pan-dystrophin
Human Dystrophin / LaminA/C
Pan-dystrophin
500µm
B
Pan-dystrophin
Human Dystrophin
LaminA/C
Human Dystrophin
LaminA/C
Pan-dystrophin
20µm
C
Pax7
Pax7
Laminin
CD29
Pax7
Laminin
Pax7
CD29
20µm
D
Pax7
Laminin
Pax7
CD29
20µm
E
Percentage of Fibers
0-199
200-399
400-599
600-799
800-999
1000-1199
1200-1399
1400-1599
1600-1799
1800-1999
F
DAPI
Pax7
DAPI
Lamin A/C
DAPI
Pax7
Lamin A/C
DAPI
Pax7
Lamin A/C
Laminin
G
hDYSTROPHIN
5 Wks
DAPI
LAMIN A/C
SPECTRIN
hDYSTROPHIN
10 Wks-Reinjury
DAPI
LAMIN A/C
SPECTRIN
H
Pax7
Lamin A/C
Pax7
Lamin A/C
Pax7
Lamin A/C
Laminin
25µm

Figure S7 (related to Figure 5): Analysis of human derived fibers.

A) Representative longitudinal section of a re-injured muscle evaluated 5 weeks after re-injury and 10 weeks after human muscle stem cell transplantation. Top panel: staining for human Dystrophin and Lamin A/C. Human-derived muscle fibers were evaluated in continuity longitudinally in TA muscle. Long sections of human-derived fibers are apparent in which the great majority of nuclei are human-derived. The upper portion of the image shows an area without human cell engraftment. Middle panel: staining for pan-dystrophin detects fibers of both mouse and human origin. Bottom panel: merged image. The images are a composite of adjacent stitched images from the section.

B) Higher power representative images distinguishing mouse from human cells and nuclei. Mouse derived nucleus (asterisk) is negative for Lamin A/C and is present in a region that is negative for human Dystrophin. Human derived nuclei (arrows) express Lamin A/C and are within a fiber expressing human Dystrophin. Blue - DAPI

C) PAX7 satellite cells are human derived. Left – a PAX7 positive cell is shown. Middle – The sublaminar position is confirmed by Laminin staining (top) and human origin of the fiber region and the satellite cell (arrow) by human CD29 staining (bottom). Right – Merged images. The distinction between laminin staining of the basement membrane indicating the sublaminar position of the satellite cell and circumferential CD29 staining of the satellite cell is evident.

D) Additional example of a human derived satellite cell after reinjury. The distinct patterns of Laminin and human CD29 staining together confirm the human origin and the sublaminar position of the cell.

E) Comparison of fiber areas of engrafted human myofibers after human CD56+/CD29+ cell transplantation. The area of all human SPECTRIN-positive muscle fibers in irriadiated NSG TA after transplantation with 5,000 CD56+/CD29+ cells from the latissimus dorsi muscle of a 64-year-old man was measured at 5 weeks (black bar), 10 weeks (gray bar) and 10 weeks, notexin

reinjury (white bar). The y axis is the percent of human fibers, the x-axis is the range of fiber area (um^2). Each bar represents the percent of engrafted human fibers of the transplant group that falls in the area range. Measured average NSG host- muscle fiber area is 2273.6±833.6um^2, measured average muscle fiber area of the same donor muscle is 5752.3±1330.5um^2. Average fiber area for 5 weeks is 253.9±128.8um^2, average fiber area for 10 weeks is 611.0±454.5um^2, average fiber area for 10 weeks-reinjury is 303.3±205.4um^2.

F) Example of human satellite cell identified by co-staining with Pax7 and human Lamin a/c. Section is from TA muscle harvested at 5 weeks after transplantation of 5,000 CD56+/CD29+ human cells (from experiment shown in figure 5B). Laminin staining was used to confirm sublaminar position of the Pax7 human cell. Scale bar 25µm.

G) Correlation of human Dystrophin expression with human Spectrin at 5 weeks and after re-injury (10 weeks). Adjacent sections to those shown in Figure 5B and C were stained with human Spectrin antibody. Scale bar 100µm.

H) Satellite cells within the transplanted muscle after reinjury (10 weeks). Sections were immunostained for PAX7, human Lamin A/C and Laminin. Representative area shows sublaminar PAX7 cells that express human Lamin A/C (arrows). A centrally located Lamin A/C nucleus that does not express PAX7 is visible as well. 70/70 analyzed PAX7 cells expressed Lamin A/C and host PAX7 satellite cells were not detected either within or outside of areas of human cell engraftment.

Supplemental Tables

Table S1: Analysis of PAX7 cells of diverse human muscles (related to Figure 1).

Muscle	Donor demographic	Number of fibers analyzed	Length of fibers analyzed (mm)	Number of PAX7 cells counted	Number of fibers per mm^2	Number of PAX7 cells per mm^3
Rectus Abdominis	40 F	10	57.6	225	197.3	771
Rectus Abdominis	45F	11	75.6	197	284.0	740
Rectus Abdominis	52 F	10	76.5	228	218.7	652
Rectus Abdominis	74M	10	199.8	333	401.6	669
Rectus Abdominis	56M	10	56.7	206	122.7	446
Rectus Abdominis	28F	11	174.9	620	649.6	2303
Rectus Abdominis	44F	10	67.2	806	35.1	421
Sartorius	62M	14	1138.6	194	2350.8	401
Sartorius	69M	10	1308.6	130	2931.2	291
Sartorius	82F	10	75.6	213	260.0	732
Sartorius	72M	10	80.4	266	164.0	543
Sartorius	85M	10	80.85	208	154.7	398
Sartorius	70F	11	80.55	258	218.7	700
Sartorius	48F	10	117.9	393	350.2	1167
Vastus Lateralis	59M	10	77.1	229	217.3	645
Vastus Lateralis	56F	10	63.75	158	220.0	545
Vastus Lateralis	66M	10	61.2	124	226.7	459
Vastus Lateralis	55F	10	64.2	167	210.7	548
Vastus Lateralis	46F	10	72.6	215	257.3	762
Pectoralis Major	55F	10	54.6	103	293.3	553
Pectoralis Major	49F	10	60	98	371.9	607
Pectoralis Major	43F	10	61.8	131	389.4	825
Pectoralis Major	44F	10	107.4	238	318.7	706
Pectoralis Major	44F	10	97.8	163	320.7	534
Pectoralis Major	51F	10	143.4	348	269.3	654
Latissimus Dorsi	68M	30	172.2	316	232.0	426
Latissimus Dorsi	50F	10	71.7	267	172.0	641
Latissimus Dorsi	83M	10	86.1	211	173.3	425
Latissimus Dorsi	39F	10	61.2	209	144.0	492
Latissimus Dorsi	60M	10	106.8	397	226.7	843
Latissimus Dorsi	54M	10	111	351	229.2	725
Gracilis	11F	10	140.7	237	213.3	359
Gracilis	65M	10	176.1	277	189.3	298
Gracilis	72M	10	88.8	177	328.0	654
Gracilis	45F	10	89.4	409	142.7	653
Gracilis	72M	10	129.6	509	194.7	765
Temporalis	19F	10	47.4	155	238.7	780
Temporalis	33M	10	75	254	288.0	975
Temporalis	27F	10	69	274	333.3	1324
Temporalis	33M	10	105	324	357.4	1103
Temporalis	58M	10	78.6	714	250.7	2277
Temporalis	54M	10	77.4	283	180.0	658
Temporalis	44M	10	57.6	206	228.2	816

The human muscle type and the donor's age and sex for each sample analyzed for PAX7 frequency are shown along with the number of fibers analyzed, their aggregate length and the number of PAX7 cells identified. Fiber content (number of fibers per mm) and the PAX7 cell content (number of PAX7 cells per mm^3) for each sample are also shown. Satellite cell content is calculated by the formula: PAX7 cells per mm^3 = number of myofibers per mm^2 x PAX7 cell frequency per mm myofiber.

Table S2: Frequency of PAX7, CD56 and CD29 cells along a fiber of different human muscles (related to Figure 1).

	Number of PAX7 cells counted/mm of fiber analyzed	Number of CD56 cells counted/mm of fiber analyzed	Number of CD29 cells counted/mm of fiber analyzed	PAX7 cells per mm	CD56 cells per mm	CD29 cells per mm
Rectus Abdominis, 52F	288/76.5	207/73.8	298/86.4	2.98	2.8	3.45
Rectus Abdominis, 28F	620/174.9	293/85.5	290/70.8	3.54	3.43	4.1
Latissimus Dorsi, 83M	211/86.1	207/102.3	312/90.6	2.45	2.49	3.44
Latissimus Dorsi, 54M	351/111	246/72.6	252/66	3.18	3.05	3.92
Sartorius, 48F	393/117.9	348/114	275/70.2	3.33	3.39	3.82
Vastus Lateralis, 56F	158/63.7	217/84.6	239/82.2	2.48	2.57	2.91

A subset of muscle samples were stained separately for PAX7, CD56 and CD29. The muscle type, and the donor's age and sex for analyzed samples are shown. For each sample, a total of 30 fibers was analyzed (10 fibers analyzed for PAX7, 10 fibers analyzed for CD56 and 10 fibers analyzed for CD29). The aggregate length of the fibers analyzed as well as the number cells positive for each marker is shown. Right 3 columns show the frequency of PAX7, CD56 and CD29 cells for each sample.

Table S3: Comparison of estimated and predicted human satellite cell content on isolated myofibers (related to Figure 2).

Aggregate length of fibers transplanted (mm)	15
Theoretical PAX7 frequency (cells/mm)	4.7
PAX7 Cell Count Fiber 1	18
PAX7 Cell Count Fiber 2	12
PAX7 Cell Count Fiber 3	9
PAX7 Cell Count Fiber 4	15
PAX7 Cell Count Fiber 5	17
PAX7 Cell Count Fiber 6	14
PAX7 Cell Count Fiber 7	11
PAX7 Cell Count Fiber 8	12
PAX7 Cell Count Fiber 9	15
PAX7 Cell Count Fiber 10	9
PAX7 Cell Count Fiber 11	9
Actual number of PAX7 cells transplanted	70
Theoretical number of PAX7 cells transplanted	64

A rectus abdominis biopsy from a 64-year-old woman was digested with collagenase and single myofibers were isolated. Five fibers of equal length were transplanted (results shown in Table 1). Eleven fibers of equal length as transplanted fibers were fixed and stained for PAX7 and LAMININ and the number of sublaminar PAX7-positive nuclei were counted (representative image shown in Figure 2B). The PAX7 count for each fiber is listed and the estimated number of satellite cells transplanted is determined by the average of the satellite cells counted from those 11 fibers multiplied by 5. The predicted satellite cell content is determined by the average PAX7 cell frequency per mm fiber (Table S1) multiplied by aggregate fiber length transplanted (15mm).

Table S4: Comparison of theoretical human satellite cell yield and actual human satellite cell yield after FACS sorting (related to Figure 4).

Muscle	Sort time after biopsy	Sample Volume (cm^3)	Actual CD56+/CD29+ cell yield	Theoretical CD56+/CD29+ cell yield
Rectus Abdominis, 64M	Day 1 After Biopsy	1.02	7,389	800,000
Vastus Lateralis, 81M	Day 1 After Biopsy	5	73,833	2,960,000
Vastus Lateralis, 69M	Day 1 After Biopsy	6	103,586	3,552,000
Vastus Lateralis, 40M	Day 1 After Biopsy	8	118,969	4,736,000

The volume of muscle tissue from 4 different muscles from 4 individuals was measured before the samples underwent digestion for FACS sorting. The total number of live CD56+/CD29+ cells obtained during the sort was recorded (actual cell yield) for each sample. To calculate the theoretical yield, the volume of each muscle was multiplied by the average of the measured satellite cell content (Table S1) for that muscle (theoretical cell yield).

Supplemental Experimental Procedures

Animal Care and Transplantation Studies

All mice were bred and housed in a pathogen-free facility at the University of California San Francisco. All procedures were approved and performed in accordance with the University of California San Francisco Institutional Animal Care and Use Committee. All experiments were performed in NOD.Cg-Prkdcscid Il2rgtm1Wjl/SzJ (NSG) mice (The Jackson Laboratory). NSG mice were pretreated with 18 gamma (Gy) or 12 Gy radiation on the day of transplantation. NSG mice exposed to 18Gy limited to the hindlimb occasionally developed ulcerations of the skin. These were treated with ointment per UCSF LARC protocols. A 1 cm incision was made in the mouse skin overlying the TA muscle and human cells or myofiber preparations were injected along with notexin (0.1ug in 50uL HBSS) (Latoxan) or 50ul 0.5% bupivacine directly into the muscle of one leg. For cell injection a 27 ½ gauge needle on a 1 cc syringe was used and for fiber transplantation a 21 gauge needle on a 1 cc syringe was used. The skin was closed with sutures and skin glue was applied over the incision. Transplanted TA muscles were harvested immediately, 1 week, 5 weeks or 10 weeks after transplantation. At 5 weeks post-transplant, some mice were reinjured with notexin (0.1ug) (Latoxan) and analyzed 5 weeks post reinjury. Harvested muscles were frozen in isopentane chilled in liquid nitrogen. Serial 10 µm transverse sections of the whole muscle were analyzed.

Human Myoblast Preparation

Frozen human myoblasts (Gibco, Cat#A12555) were thawed and plated onto 0.1% gelatin coated tissue culture treated flasks in growth medium (DMEM, 20% FBS, l-glut, sodium pyruvate, supplemented with antibiotics) containing 5ng/ml basic fibroblast growth factor (R&D Systems, Minneapolis, MN). Medium was changed every two days until the myoblasts reached an 80% confluence after which the myoblasts were passaged. Myoblasts were transplanted at p2, mpd 13 - 14.

Human Muscle Analysis

After procurement, human muscle samples were split for analysis. Part of the specimen was immediately fixed in 4% paraformaldehyde (PFA) at room temperature for 10 min and washed with PBS. The sample was then embedded in glycerol. For this, the sample was first placed in 30% glycerol in PBS overnight at 4°C, then 50% glycerol in PBS overnight at 4°C, then 80% glycerol in PBS overnight at 4°C and finally 100% glycerol. The fibers are stored in 100% glycerol at 4°C until dissection.

Single fibers were dissected using fine forceps under a dissecting microscope. Single fibers were washed in PBS for 15 min at room temperature, then permeabilized with 0.5% Triton X-100 (Sigma-Aldrich, St. Louis, MO) for 6 min, and washed with PBS for 15 min. Single fibers were then blocked with 10% goat serum in PBS for 30 min at room temperature and incubated overnight at 4°C with the following primary antibodies: mouse monoclonal anti-PAX7 (1:25 Developmental Studies Hybridoma Bank, Cat# PAX7), anti-human CD29 (1:25, Serotec Cat# MCA2028) (Figure 1), or FITC-conjugated anti-CD56 (1:25 NCAM16.2, BD Biosciences, Cat# 340410) and rabbit polyclonal anti-LAMININ (1:25, Sigma-Aldrich Cat# L9393) diluted in PBS containing 10% normal goat serum. After PBS wash at room temperature for 15 min, the following corresponding secondary antibodies were applied for 1 hr at room temperature: Alexa Fluor 488 goat anti-mouse IgG (1:500 Invitrogen, Cat# A-11001), Alexa Fluor 555 goat anti-rabbit IgG (1:500Invitrogen, Cat# A-21428). Fibers were washed in PBS for 15 min twice and then mounted with VECTASHIELD mounting medium with DAPI (Vector Laboratories Cat# H-1200) and all samples were examined using a Leica upright microscope.

The remaining portion of the sample that was not fixed was frozen in isopentane chilled in liquid nitrogen. Transverse 6 or 10 µm cross sections were obtained. Sections were thawed at room temperature for 15 min.

For hematoxylin and eosin (H&E) staining, slides with 10 µm cross sections were rinsed with water and dried. Sections were then dehydrated as follows; 5 min in xylenes, twice; 5 min in 100% ethanol, twice; 5 min in 95% ethanol; 5 min in 80% ethanol and washed in water for 30 s. Slides were then placed in 3x Gill's Hematoxylin for 4 min and washed with water for 30 s. For nuclear staining, slides were placed in Scott's water for 3 min and washed in water for 30 s. Slides were then placed in Eosin for 2 min and washed with water for 30 s. Sections were dehydrated again as follows: 1 min 80% ethanol; 2 min 95% ethanol, twice; 3 min 100% ethanol, twice; 2 min xylenes, twice. Slides were then mounted with Permount and coverslips and air dried overnight before imaging. All samples were examined using a Leica upright microscope and muscle area was analyzed using ImageJ (ImageJ, U. S. National Institutes of Health, Bethesda, Maryland, USA, http://imagej.nih.gov/ij/, 1997-2014).

For antibody staining the slides with 6-10 µm cross sections were fixed in 2-4% PFA at room temperature for 5-10 min, washed in PBST (PBS+ 0.1% Tween 20 (Sigma-Aldrich, St. Louis, MO)), blocked with DAKO Protein Block (Cat# X0909) and incubated at room temperature overnight with the following primary antibodies: mouse monoclonal anti-PAX7 (1:25 Developmental Studies Hybridoma Bank, Cat# PAX7), Alexa Fluor 647-conjugated anti-human CD29 TS2/16 (1:50 BioLegend, Cat# 303018) (figures 3, 4G, S2, S7), rabbit monoclonal anti-CD56 (1:100 abcam, Cat# ab75813) (Figures 1, S2 top and 3C), mouse monoclonal anti-CD56 (1:10 BD Biosciences Cat# 555515) (Figure S3), rabbit polyclonal anti-MYOD (1:200, Santa Cruz Biotechnology, Cat# sc-760), rabbit polyclonal anti-MYF5 (1:200 Santa Cruz Biotechnology, Cat# sc-302), mouse monoclonal anti SMA (1:400 Sigma Cat# C6198), rabbit anti PDGFRb (1:100 Cell Signaling Cat# 3169), rabbit anti NG2 (1:100 Millipore Cat# AB5320),

rabbit polyclonal anti-LAMININ (1:25 Sigma-Aldrich, Cat# L9393) or chicken polyclonal anti-LAMININ (1:1000 abcam, Cat# ab14055,) diluted in DAKO Antibody Diluent (DAKO Cat# S0809). After PBST wash for 3 min 3 times, the following corresponding secondary antibodies were applied for 1 hr at room temperature: FITC-conjugated donkey anti-mouse (1:300 Jackson Immunology,Cat# 715-095-150), Cy3-conjugated donkey anti-mouse (1:500 Jackson Immunology, Cat# 715-165-150), Cy5-conjugated donkey anti-chicken (1:200 Jackson Immunology, Cat# 703-175-155), Cy5 donkey anti-mouse (1:200 Jackson Immunology, Cat# 715-175-150), FITC-conjugated donkey anti-rabbit (1:300 Jackson Immunology, Cat# 711-095-152) diluted in DAKO Antibody Diluent (Carpinteria Cat# S0809). Sections were mounted with VECTASHIELD mounting medium with DAPI (Vector Laboratories Cat# H-1200) and all samples were examined using a Leica upright microscope.

Isolation of Live Human Muscle Fibers

Immediately after human muscle was explanted, the sample was incubated for 1 hr in 0.2% type I collagenase (Sigma-Aldrich, St. Louis, MO) in DMEM with sodium pyruvate and placed in a shaker in a 37°C incubator. The sample was then transferred to a petri dish coated with horse serum and then washed in DMEM with sodium pyruvate supplemented with antibiotics. After wash, the sample was placed in a fresh horse-serum-coated petri dish with DMEM with sodium pyruvate supplemented with antibiotics and individual fibers were separated under a dissecting microscope using fine forceps and fiber length was measured. 5 dissected single fibers were then taken up in a 1 cc syringe with a 21 gauge needle and injected into the recipient muscle with the appropriate myotoxin. Before fibers were aspirated, 10% horse serum was passed through the needle and syringe to prevent fiber adhesion. Single fibers that were not transplanted were either fixed with 4% PFA or cultured. For fixation, dissected fibers were taken up in a 1 cc syringe with a 21 gauge needle and injected into 4%PFA and the fixed fibers were stained for PAX7 and LAMININ as described above for glycerol-embedded fibers.

For live fiber culture, individual fibers were aspirated and injected into culture media (20%FBS, 10% HS in DMEM with sodium pyruvate supplemented with antibiotics). Culture medium was changed every 2 days. After being in culture medium for 2 weeks, wells were either fixed with 4% PFA or switched to differentiation medium (DMEM F12, 2% HS) for 7 days. Differentiation medium was changed daily. After 7 days, cells were fixed with 4% PFA. All fixed cells were washed with PBS for 15 min and then permeabilized with 0.5% Triton X-100 (Sigma-Aldrich, St. Louis, MO) for 6 min. After PBS wash for 15 min they were blocked with 10% goat serum in PBS and incubated for 1 hr at room temperature with the following primary antibodies diluted in 10% goat serum in PBS: mouse monoclonal anti-myosin heavy chain (1:100 Novus Biologicals, Cat# NB300-284, Littleton, CO) or rabbit polyclonal anti-MYOD (1:200 Santa Cruz Biotechnology, Cat# sc-760). Cells were then washed in PBS for 15 min and the following secondary antibodies diluted in 10% goat serum in PBS were applied for 1 hr at room temperature: Alexa Fluor 488 goat anti-mouse IgG (1:500, Invitrogen, Cat# A-11001) or Alexa Fluor 555 goat anti-rabbit IgG (1:500, Invitrogen Cat# A-21428). Wells were mounted with VECTASHIELD mounting medium with DAPI (Vector Laboratories, Cat# H-1200) and all samples were examined using a Leica inverted microscope.

Cell preparation from human muscle biopsies

Freshly harvested human muscle was either immediately digested or stored overnight in 30% FBS at 4°C. At the time of digestion, samples were finely minced with scalpels and incubated in Pronase (1mg/ml, Sigma-Aldrich, St. Louis, MO) in 1% HEPES for 1 hr in a shaker in a 37°C incubator. The tissue was triturated and then centrifuged at 150 g for 2 min. The supernatant was collected and washed in 20% FBS in DMEM. The cells were then centrifuged at 1000 g for 5 min at 4°C. The supernatant was then discarded and the cell pellet stored on ice in 20% FBS in DMEM.

Undigested tissue after Pronase digestion underwent a second digestion in Collagenase XI (1mg/ml Sigma-Aldrich, St. Louis, MO) in 5%FBS in DMEM for 30 min on a shaker in a 37°C incubator. After collagenase digestion, the tissue was triturated and centrifuged at 100g for 2 min. The supernatant was then collected and washed with 20%FBS in DMEM and centrifuged at 1000g for 5 min at 4°C. The supernatant is then discarded and cell pellet is reconstituted with 20% FBS in DMEM and combined with cells from the Pronase digestion

The cells were then filtered through a 100 µM cell strainer followed by filtration through a 40µM cell strainer. The cells were then centrifuged at 1000g for 5 min at 4°C. The supernatant was discarded and the cell pellet underwent erythrocyte lysis by incubation with ACK buffer with 5% FBS for 8 min on ice. After lysis, the remaining cells were washed with cold PBS. If erythrocytes were still seen, the cells underwent a second round of erythrocyte lysis. After wash in PBS the cells were centrifuged at 1000g for 5 min at 4°C. The supernatant was aspirated and the cells were taken up in FACS buffer (HBBS, 2% FBS and 2 mM EDTA (Sigma-Aldrich, St. Louis, MO)).

Some digested human muscle cells were then stained with an antibody cocktail consisting of Pacific Blue-conjugated anti-human CD31 (1:25 BioLegend Cat# 303114), Alexa Flour 700-conjugated anti-human CD45 (1:50 BioLegend, Cat# 304024), Alexa Fluor 488-conjugated anti-human CD29 (1:20 BioLegend, Cat# 303016), and PE-conjugated anti-human CD56 (1:10 MY31 BD Biosciences Cat# BD347747) for 45 min on ice. The remaining cells were stained with the following isotype control antibodies for gating: FITC-conjugated anti-mouse IgG1 (1:20 BioLegend, Cat# 406605), PE-conjugated anti-mouse IgG2 (1:10 MY31 BD Biosciences Cat# BDB550085), Alexa Fluor 700-conjugated anti-mouse IgG1 (1:50 BioLegend, Cat# 400144) and Pacific Blue-conjugated anti-mouse IgG1 (1:25 BioLegend, Cat# 400151San Diego, CA). After antibody incubation, the cells were washed with cold FACS buffer and centrifuged at 700g for 5 min at 4°C for three times. After the last wash the cells were taken up in 200µl FACS buffer with 7AAD (1:1000 BioLegend, San Diego, CA)

Satellite cell sorting

All flow cytometry analysis and cell sorting were performed at the University of California San Francisco Flow Cytometry Core with the BD FACSAria2 operated using FACS Diva software. Viable cells were gated using 7AAD and singlet cells were based on scattering to avoid cell clusters. First, cells incubated with isotype antibodies were analyzed to determine gating. Then viable cells were depleted for CD45 and CD31 expressing cells. Cells that remained after depletion were sorted for CD56+/CD29- and CD56+/CD29+ and collected for further experimentation. Cells to be transplanted were taken up in 50ul of 20%FBS in DMEM supplemented with 10 µM Rho-associated protein kinase inhibitor (ROCKi).

Pax7 immunostaining of cells from digested muscle

Anti-Pax7 antibody was purified by protein A –sepharose affinity from Pax7 hybridoma (DSHB) supernatant using standard protocols. The Pax7 antibody was directly conjugated using Alexa-fluor-350 carboxylic acid succinimide (Life Technologies). Sorted cells were collected in 20%FBS-DMEM with 10 mM ROCKi and plated directly into wells of BioCoated laminin-coated chamber slides (BD Biosciences) previously coated for 1 hr with extracellular matrix gel (1:100, Sigma-Aldrich) in F12/DMEM. The cells were incubated in the chamber slides for 1 hr at 37^{o}C with 5% CO2 to allow for attachment. The cells were washed with PBS and then fixed in 4% PFA for 20 min. The fixed cells were place in pre-heat (95^{o}C) target retrieval solution (Dako) for 20 min then allowed to cool to room temperature. Cells were blocked with 5% Goat Serum in 0.3% Triton X-PBS and incubated with directly conjugated anti-Pax7-Alexa fluor-350 O/N. Cells were counterstained with Sytox-orange (Life Technologies) and mounted in Vectashield without DAPI. Photos were taken on confocal microscope and pseudocolored.

qRT-PCR

RNA was extracted from cells using the RNeasy Mini Kit including DNase treatment (Qiagen, Valencia, CA) according to the manufacturer's instruction. RNA concentration was measured using a Nanodrop ND-1000 Spectrophotometer (Thermo, Waltham, MA) to convert equal quantities of mRNA into cDNA using the Superscript™ III First-Strand Synthesis System (Invitrogen, Carlsbad, CA). Relative gene expression was determined using TaqMan Assay (Applied Biosytems, Carlsbad, CA) on an ABI 7300 Real-Time PCR system with the human primer pair PAX7 (Hs00242962m1). Cycle threshold (Ct) value for detecting a gene of interest was normalized against Ct value of the housekeeping gene, human GAPDH (Applied Biosystems, Cat# 4333764F), and relative changes were calculated according the ΔΔCt method.

NSG TA analysis

All glass slides were removed from -80°C and warmed at room temperature for 10 min. H&E staining was performed as described above for human sections.

For human LAMIN A/C and human SPECTRIN immunostaining, NSG sections were fixed in 4% PFA for 10 min at room temperature and then washed with PBS for 3 min 3 times and then permeabilized with 0.5% Triton X-100 (Sigma-Aldrich, St. Louis, MO) for 6 min. The sections were then washed for 3 min with PBS 3 times and blocked with 10% goat serum in PBS for 30 min at room temperature. The sections were then incubated for 1 hr at room temperature with the following primary antibodies: mouse monoclonal anti-human SPECTRIN (1:100 Leica Microsystems, Cat# NCL-SPEC1 Buffalo Grove, IL) and mouse monoclonal anti-human LAMIN A/C (1:100 Vector Laboratories, Cat# VP550 Burlingame, CA) in 10% normal goat serum in PBS. The sections were then washed for 3 min with PBS 3 times followed by 30 min of incubation at room temperature with Alexa Fluor 488 goat anti-mouse IgG (1:500, A-11001 Invitrogen, Carlsbad, CA) in 10% normal goat serum in PBS. Sections were mounted with

VECTASHIELD mounting medium with DAPI (H-1200 Vector Laboratories, Burlingame, CA) and all samples were examined using a Leica upright microscope.

For all other immunostainings, the slides were fixed in 2% PFA at room temperature for 10 min, washed in PBST (PBS+ 0.1% Tween 20 (Sigma-Aldrich, St. Louis, MO)), and then blocked with DAKO Protein Block (X0909 Carpinteria, CA) and incubated at room temperature overnight with the following primary antibodies: mouse monoclonal anti-PAX7 (1:20 DHSB, Iowa City, Iowa), chicken polyclonal anti-pan laminin (1:25 abcam, Cat# AB14055), rabbit polyclonal anti-pan dystrophin (1:500 Thermo, Cat# PA5-16734), mouse monoclonal anti-human DYSTROPHIN clone Dy10/12B2 (1:25 Leica Microsystems Cat# NCL-DYS3), Alexa Fluor 647-conjugated anti-human CD29 clone TS2/16 (1:50 BioLegend, Cat# 303018), rabbit monoclonal anti-CD56 (1:100 abcam Cat# ab75813), rabbit polyclonal anti-MYOD (1:200 Santa Cruz Biotechnology, Cat# sc-760), rabbit polyclonal anti-MYF5 (1:200, Santa Cruz Biotechnology, Cat# sc-302), or chicken polyclonal anti-laminin (1:1000 abcam, Cat# AB-14055, Cambridge, MA), Alexa Fluor 555-conjugated anti α-bungarotoxin (1:500 Invitrogen, Cat# B35451), rabbit polyclonal anti-synaptophysin (1:100 DAKO, Cat# A 0010) diluted in DAKO Antibody Diluent (DAKO, Cat# S0809). After PBST wash for 3 min 3 times, the following corresponding secondary antibodies were applied for 1 hr at room temperature: FITC donkey anti-mouse (1:300 Jackson Immunology, Cat# 715-095-150), Cy3 goat anti-mouse (1:500 Jackson Immunology,), Cy5 donkey anti-chicken (1:200 Jackson Immunology, Cat# 7053-175-155), Cy5 donkey anti-mouse (1:200 Jackson Immunology, Cat# 715-175-150), FITC donkey anti-rabbit (1:300 Jackson Immunology, Cat# 711-095-152). Sections were mounted with VECTASHIELD mounting medium with DAPI (H-1200 Vector Laboratories, Burlingame, CA) and all samples were examined using a Leica upright microscope.